SeaWiFS Ocean Aerosol Retrieval (SOAR): Algorithm, validation, and comparison with other data sets

A. M. Sayer,[1,2] N. C. Hsu,[2] C. Bettenhausen,[2,3] Z. Ahmad,[2,4] B. N. Holben,[2] A. Smirnov,[2,5] G. E. Thomas,[6] and J. Zhang[7]

Received 22 July 2011; revised 28 October 2011; accepted 7 November 2011; published 15 February 2012.

[1] The Sea-viewing Wide Field-of-view Sensor (SeaWiFS) provides a well-calibrated 13-year (1997–2010) record of top-of-atmosphere radiance, suitable for use in retrieval of atmospheric aerosol optical depth (AOD). This paper presents and validates a SeaWiFS Ocean Aerosol Retrieval (SOAR) algorithm, which retrieves the AOD at 550 nm and the partition of aerosol particle volume between fine and coarse modes. The algorithm has been applied over water to the whole SeaWiFS record. The data set includes quality flags to identify those retrievals suitable for quantitative use. SOAR has been validated against Aerosol Robotic Network (AERONET) and Maritime Aerosol Network (MAN) data and found to compare well (correlation 0.86 at 550 nm and 0.88 at 870 nm for AERONET, and 0.87 at 550 nm and 0.85 at 870 nm for MAN, using recommended quality control settings). These comparisons are used to identify the typical level of uncertainty on the AOD, estimated as 0.03 + 15% at 550 nm and 0.03 + 10% at 870 nm. The data set also includes the Ångström exponent, although as expected this is noisy for low aerosol loadings (correlation 0.50; 0.78 for points where the AOD at 550 nm is 0.3 or more). Retrieved AOD is compared with colocated observations from other satellite sensors; regional and seasonal patterns are found to be common between all data sets, and differences generally linked to factors such as cloud screening and retrieval assumptions.

Citation: Sayer, A. M., N. C. Hsu, C. Bettenhausen, Z. Ahmad, B. N. Holben, A. Smirnov, G. E. Thomas, and J. Zhang (2012), SeaWiFS Ocean Aerosol Retrieval (SOAR): Algorithm, validation, and comparison with other data sets, *J. Geophys. Res.*, *117*, D03206, doi:10.1029/2011JD016599.

1. Introduction

[2] To improve understanding of radiative forcing of the Earth system, of which the largest current uncertainties relate to the direct and indirect radiative effects of aerosols [*Forster et al.*, 2007; *Stevens and Feingold*, 2009], long-term accurate and stable climate data records (CDRs) of a range of essential climate variables (ECVs) are necessary [*Global Climate Observing System* (*GCOS*), 2009, 2010]. The primary purpose of the Sea-viewing Wide Field-of-view Sensor (SeaWiFS) was retrieval of ocean color parameters, for which a high quality of radiometric accuracy was required and maintained over its 13-year (1997–2010) lifetime [*McClain et al.*, 2004]. Although new, advanced sensors will be required to address some of the requirements for CDRs in full, the combination of a long (on satellite timescales) time series and high quality of calibration mean that SeaWiFS is well-suited for the generation of a historical aerosol data set. In particular, the launch in 1997 predates that of the Terra, A-Train and Envisat platforms also used for aerosol remote sensing, and encompasses much of the strong 1997–1998 El Niño event.

[3] The aim of the Deep Blue Utilization of SeaWiFS Through the Data and Information Services Center (DUST-DISC) project is to develop the SeaWiFS record to create a stable aerosol optical depth (AOD) archive. The information content of past and current satellite measurements is insufficient to retrieve unambiguously all aerosol parameters of interest [*Hasekamp and Landgraf*, 2007; *Mishchenko et al.*, 2007; *Kokhanovsky et al.*, 2010]. Therefore, aerosol data sets created from satellite measurements adopt constraints, typically linked to aerosol microphysical properties and surface reflectance, dependent upon the particular characteristics of each sensor. As such, retrieval algorithms are optimized for individual sensors (although they often share conceptual similarities).

[4] This study describes and validates the SeaWiFS Ocean Aerosol Retrieval (SOAR) algorithm, used to retrieve spectral AOD over water, in the DUST-DISC project. The over-land AOD retrieval provides coverage over both vegetated and desert surfaces, and draws on the heritage of the ‘Deep

[1]Goddard Earth Sciences Technology and Research, Universities Space Research Association, Columbia, Maryland, USA.
[2]NASA Goddard Space Flight Center, Greenbelt, Maryland, USA.
[3]Science Systems and Applications, Inc., Lanham, Maryland, USA.
[4]Science and Data Systems, Inc., Silver Spring, Maryland, USA.
[5]Sigma Space Corporation, Lanham, Maryland, USA.
[6]Atmospheric, Oceanic, and Planetary Physics, University of Oxford, Oxford, UK.
[7]Department of Atmospheric Science, University of North Dakota, Grand Forks, North Dakota, USA.

0148-0227/12/2011JD016599

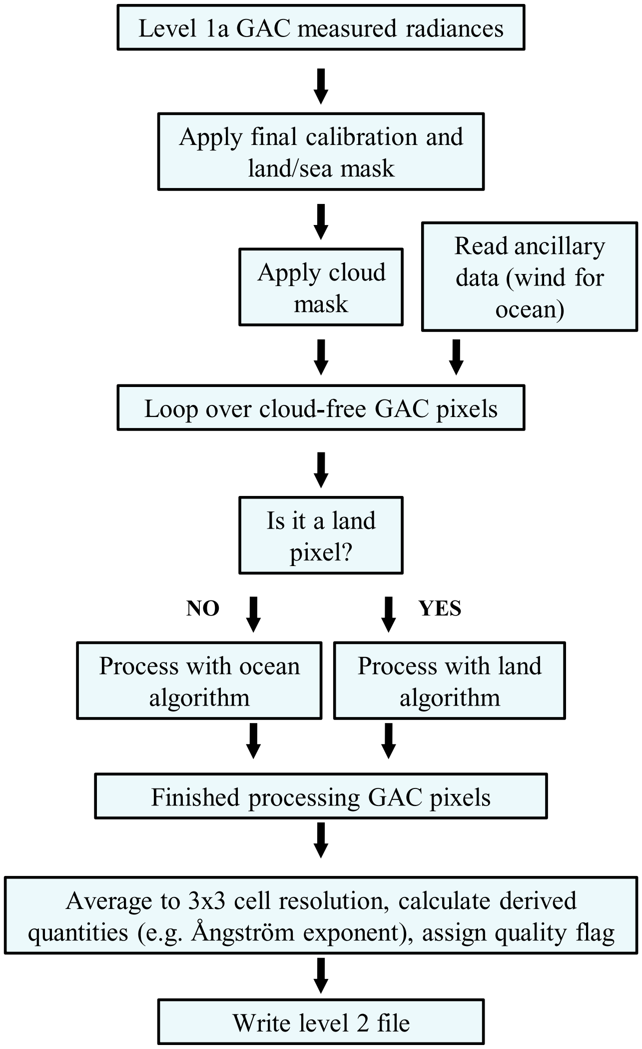

Figure 1. Flowchart summary of SeaWiFS retrieval processing chain.

Blue' algorithm [*Hsu et al.*, 2004, 2006], which is part of the operational MODerate Resolution Imaging Spectroradiometer (MODIS) processing, and will be described in a forthcoming publication. The data set created using these algorithms is freely available from http://disc.gsfc.nasa.gov/dust/ along with supporting documentation for users. The most recent processing of the data set, described in this work, is version 3.

2. Overview of SeaWiFS and SOAR

[5] SeaWiFS measured top-of-atmosphere (TOA) reflected solar radiance in bands centered near 412, 443, 490, 510, 555, 670, 765, and 865 nm. A high signal-to-noise ratio (≥600–1100 when viewing the solar diffuser) and stable calibration were maintained for all bands; the largest uncertainty (2%–3%) was the absolute calibration [*Eplee et al.*, 2007, 2011; *Franz et al.*, 2007]. The sensor was launched in a Sun-synchronous orbit at an altitude of 705 km and inclination of 98.25°, with a nominal local solar time around 12 pm for the sub-satellite point for the descending (daytime) orbit node. This drifted through the mission, although remained between 12 pm and 12:30 pm until 2005, and reached a maximum around 2:40 pm in mid-2010.

[6] Full spatial resolution at the sub-satellite point was 1.1 km × 1.1 km, known as local area coverage (LAC) mode. Due to data capacity limitations, LAC data are only available for limited regions. Global Area Coverage (GAC) mode consisted of LAC pixels subsampled on-board the satellite with gaps of 4 pixels between each; thus, each GAC pixel is a measurement of a 1.1 km × 1.1 km field of view taken to represent an area of approximately 4.5 km × 4.5 km (both resolutions quoted for the sub-satellite point). The swath width of GAC data is 1,502 km, with 15 or 16 orbits per day, providing daily coverage outside the tropics, and near-daily coverage in the tropics. As it is designed for global application, only GAC data are used in the SOAR algorithm. Therefore, from this point, the term 'pixel' refers to the data at GAC resolution. SeaWiFS was tilted off-nadir to decrease exposure to sun-glint over the oceans, meaning that the typical range of viewing zenith angles was from 20° at the center of the swath to 60° at the edge (and consequently pixel area increases by a factor of approximately 4 at the edge of the swath relative to the center).

[7] The SOAR algorithm is divided into three phases: a preprocessing step during which instrument pixels affected by clouds are identified; the aerosol retrieval itself; and a postprocessing stage where individual retrievals are aggregated to coarser resolution, and quality flags are assigned. A summary flowchart is shown in Figure 1.

[8] The algorithm retrieves two parameters. The first is the AOD (denoted τ_λ, where λ is the wavelength in nm). The AOD retrieved by the algorithm is τ_{550}, and unless specified otherwise through this work the term AOD refers to τ_{550}. The second is the partition between the fine and coarse aerosol modes used in the aerosol retrieval, presented as the fine mode volume fraction (f_f), such that $f_\mathrm{f} = 0$ indicates a pure coarse-mode distribution and $f_\mathrm{f} = 1$ a pure fine-mode one. Other quantities of interest, such as the AOD referenced to other wavelengths, or the Ångström exponent, may be derived from these. Assumptions about the radiative properties of aerosol particles are required for the retrieval, which are detailed in Section 2.3. Retrieving both an AOD and a weighting parameter between modes is similar to the approach of MODIS over ocean [*Tanré et al.*, 1997]. This approach has been used to, for example, study the partition between marine, dust, and biomass burning aerosols transported across the Atlantic Ocean [*Kaufman et al.*, 2005], and highlights the additional utility of size-related aerosol data, as opposed to just single-wavelength AOD.

2.1. Preprocessing

[9] As a first step, Level 1a GAC files (individual orbit swaths) are converted to Level 1b format using the SeaDAS software package version 6.2 (available at http://seadas.gsfc.nasa.gov/), which applies final calibration to the radiance data. Then, the radiance in each band (L^r) is divided by the incident solar irradiance at nadir (E^i, taken from *Thuillier et al.* [2003]) to give the sun-normalized radiance ρ_TOA, where

$$\rho_\mathrm{TOA}(\theta_\mathrm{s}, \phi_\mathrm{s}; \theta_\mathrm{v}, \phi_\mathrm{v}) = \frac{\int_{\lambda_1}^{\lambda_2} L^r(\theta_\mathrm{s}, \phi_\mathrm{s}; \theta_\mathrm{v}, \phi_\mathrm{v}; \lambda)\xi(\lambda)d\lambda}{\int_{\lambda_1}^{\lambda_2} E^i(\lambda)\xi(\lambda)d\lambda}. \quad (1)$$

Here, $\xi(\lambda)$ is the band's spectral response function defined between wavelengths λ_1 and λ_2, and the wavelength-dependence of ρ_{TOA} is omitted for simplicity of notation. Zenith angles are denoted θ and azimuth ϕ; subscripted s indicates a solar angle, and v a satellite ('viewing') angle.

[10] Near-surface (10 m) wind fields, obtained from the National Center for Environmental Prediction (NCEP) reanalyses [*Derber et al.*, 1991], are read in. These are available at 1° × 1° latitude and longitude resolution and 6-hour temporal resolution, and are linearly interpolated in space and time for each pixel. A land-sea mask is used to determine whether the SOAR algorithm is applied or not.

[11] Pixels identified as being cloudy are not processed with the SOAR algorithm. An over-water pixel is marked as cloudy if the standard deviation of ρ_{TOA} at 412 nm over a 3 × 3 pixel window around it is larger than $0.3\cos\theta_s$. This test has been found to be effective as cloud fields are bright and typically inhomogeneous while dark clear-sky oceans have lower variability [*Martins et al.*, 2002]. Additionally, it was found to be robust even in cases of high AOD. Unfortunately, as SeaWiFS lacked thermal channels and only collected measurements at a static viewing geometry, standard cloud identification techniques used by other passive sensors cannot be applied. This means that clouds which are homogeneous on the order of several pixels can sometimes be missed by this test. This cloud flag also identifies most pixels covered by sea ice. Additional tests performed during assignment of quality flags (discussed in Section 2.6) are used to identify retrievals suspected of residual contamination by clouds, sea ice, or highly turbid waters.

2.2. Retrieval Technique

[12] Aerosol optical properties of interest are retrieved by inverting measured dependent quantities (here, ρ_{TOA}). The mapping between the variables of interest and these observable quantities is known as the forward function, approximated in the retrieval by a forward model (FM). The aerosol retrieval determines τ_{550} and f_f simultaneously using ρ_{TOA} measured by the SeaWiFS bands centered near 510 nm, 670 nm, and 865 nm (retrieval of two unknown quantities from three measurements).

[13] The FM is based upon linear interpolation of precalculated lookup tables (LUTs) of ρ_{TOA}. The most probable values of the aerosol optical parameters are found by minimizing the sum (over all three channels) of squared differences between measured ρ_{TOA} and LUT values. The difference between measured and modeled values is termed the residual on the fit. This strategy is similar to that employed in other AOD retrieval algorithms [e.g., *Tanré et al.*, 1997]. The Levenburg-Marquardt method [*Levenberg*, 1944; *Marquardt*, 1963] is used for minimization. As the absolute uncertainty of the measurements and FM are unknown, no scaling is applied to these residuals. This results in the 510 nm band being weighted slightly more than the others, as this channel is typically the brightest. The starting point for the iteration is taken as the LUT node point (i.e., combination of τ_{550} and f_f) with the lowest sum of square residuals.

[14] LUTs are calculated using the vector version of the Second Simulation of the Solar Signal in the Satellite Spectrum (6S) radiative transfer code [*Vermote et al.*, 1997], which is based on the 'successive orders of scattering' technique, and has an accuracy better than the SeaWiFS calibration uncertainty of 2%–3% [e.g., *Kotchenova et al.*, 2008]. The LUT contains nodes at 10 values of θ_s, 11 of θ_v, 11 of ϕ_r, 10 AODs (allowing $0.002 \leq \tau_{550} \leq 3.5$), 10 f_f, and 3 wind speeds (2 ms^{-1}, 6 ms^{-1}, and 15 ms^{-1}). AODs higher than 3.5 are unexpected over the ocean [e.g., *Smirnov et al.*, 2011]. If the wind speed for a given pixel lies outside the range of the LUT, the lower or upper limit (as appropriate) is used instead. Away from sun-glint, wind speed effects on ocean surface reflectance are negligible for low winds, while at high winds parameterizations of such effects become increasingly uncertain, and the likelihood of cloudiness increases [*Koepke*, 1984; *Anguelova and Webster*, 2006]. Therefore these limits have minimal impact on the retrieval.

[15] The 6S code allows for a bidirectional reflectance distribution function (BRDF) representation of surface reflectance in the retrieval. The ocean BRDF model in 6S draws on the method of *Koepke* [1984], which has been applied widely in satellite aerosol remote sensing [e.g., *Tanré et al.*, 1997; *Martonchik et al.*, 1998; *Sayer et al.*, 2010a]. This includes contributions from oceanic whitecaps, sun-glint, and scattering from within the water ('underlight', although this latter term is set to zero in 6S for wavelengths longer than 700 nm). Assumption of a fixed wind speed has been shown [*Zhang and Reid*, 2006; *Sayer et al.*, 2010a; *Shi et al.*, 2011] to lead to wind speed-dependent biases in satellite aerosol retrievals, which is why the LUT used is calculated for three wind speeds.

[16] Underlight in the 6S code is calculated using an empirical relationship based on chlorophyll-*a* content (*chl*). This was developed for so-called 'Case 1' waters, under the definitions adopted by the satellite ocean color community [e.g., *Morel and Prieur*, 1977]. Essentially, these are (largely open-ocean) bodies of water whose optical properties can be described adequately by their phytoplankton content, proxied by *chl* (as other optically active components of seawater covary strongly with *chl*). In the retrieval, a fixed *chl* =0.2 mg m^{-3} is assumed, which is a representative value for open oceans. Water bodies where constituents other than *chl* are necessary to model scattering and absorption are known as Case 2 (as *chl* and other substances covary less strongly, and there are additional influences from e.g. continental runoff and increased in-water turbidity), and are more commonly coastal. Case 2 waters are much more complicated to model accurately. *Jamet et al.* [2011] present comparisons between three atmospheric correction algorithms for Case 2 waters, which highlights some of these issues. Due to this and other difficulties in coastal waters (e.g. surface heterogeneity, and reflection from the ocean floor for shallow waters) performance of the retrieval is expected to be poorer in these cases.

[17] A midlatitude summer standard atmosphere [*McClatchey et al.*, 1971] is assumed for the LUT, and calculations are performed for a surface pressure of 1 atmosphere, as the variability in ρ_{TOA} due to gas or sea level pressure fluctuations (as well as changes in total column ozone) is small for the bands used. The standard 6S aerosol particle vertical profile (exponentially decreasing with a scale height of 2 km) is used. Aerosol phase functions are calculated with Mie theory.

Table 1. Locations of the AERONET Sites Used to Obtain the Aerosol Microphysical Models for High Aerosol Loadings, and Number of Such Cases at Each Site[a]

Site	Latitude (deg)	Longitude (deg)	Elevation (m Above Sea Level)	Number of Cases
Cape San Juan	18.384	−65.620	15	39
Capo Verde	16.733	−22.935	60	1173
Dakar	14.394	−16.959	0	1589
Lampedusa	35.517	12.632	45	67
La Parguera	17.970	−67.045	12	70
Santa Cruz Tenerife	28.473	−16.247	52	280
COVE	36.900	−75.710	37	314
Helgoland	6.7760	73.183	0	166
Gosan-SNU	54.178	7.8870	33	25
Kaashidhoo	4.9650	73.466	0	46
MCO Hanimaadhoo	33.292	126.162	72	168
Venise	45.314	12.508	10	552
Villefranche	43.684	7.3290	130	105

[a]The first six sites are optically dominated by their coarse mode (dust), and the last seven by their fine mode (transported pollution).

2.3. Aerosol Microphysical Models

[18] In SOAR, aerosol particles are modeled using a bimodal lognormal distribution, defined by its volume size distribution

$$\frac{dV(r)}{d\ln(r)} = \sum_{i=\mathrm{f,c}} \frac{C_{\mathrm{v},i}}{\sqrt{2\pi}\sigma_i} e^{-\frac{1}{2}\left(\frac{\ln(r)-\ln(r_{\mathrm{v},i})}{\sigma_i}\right)^2}, \tag{2}$$

which describes the volume of particles in the infinitesimal size range $r \pm d\ln(r)$, where r is the aerosol particle radius, and the distribution parameters C_v, r_v and σ denote the total volume, volume median radius, and standard deviation of each mode. Subscripted f indicates fine mode properties, and subscripted c the coarse mode. Each mode also has its own complex refractive index $m = n - ik$, where n is the real component and k the absorption coefficient, assumed spectrally neutral between the bands used. For a given r_v, σ, and m, the AOD will be dependent on total aerosol particle volume C_v. Thus, f_f is defined as $C_{\mathrm{v,f}}/(C_{\mathrm{v,f}} + C_{\mathrm{v,c}})$, and the retrieved τ_{550} and f_f could be expressed in terms of the aerosol volume size distribution (as, for a given modal radius, spread, and refractive index, the AOD for the fine mode and coarse mode are proportional to the mode volumes). The equivalent coarse-mode volume fraction is expressed simply as $f_\mathrm{c} = 1 - f_\mathrm{f}$.

[19] Three different pairs of fine and coarse mode aerosol microphysical properties are used in the LUT. First is a model for unpolluted marine aerosol, used where $\tau_{550} \leq 0.3$. Second, one of two more absorbing models are used where $\tau_{550} > 0.3$. These models are either optically dominated by fine or coarse modes, and represent a mixture of marine aerosol with transported small absorbing aerosol (such as continental pollution or biomass burning), or a mixture of marine aerosol and dust, respectively. The change in assumed properties at $\tau_{550} > 0.3$ is based on the fact that the AOD for unpolluted marine conditions is typically low [*Smirnov et al.*, 2002, 2011], i.e. elevated AODs are indications of some non-maritime contribution. The value of 0.3 is arbitrary, but small changes to this threshold were found to affect retrieved AOD by generally less than the retrieval uncertainty. Within the $\tau_{550} > 0.3$ range, the 'fine-dominated' model is used in the LUT for $f_\mathrm{f} > 0.25$ and 'coarse-dominated' otherwise.

[20] In 6S, aerosol particle optical properties are computed at twenty wavelengths throughout the solar spectrum. The spectral variability of the extinction coefficient is stored so that the retrieved values of τ_{550} and f_f can be used to calculate the AOD at the SeaWiFS bands used in the retrieval, as part of the output data product (see Section 2.6). Additionally, the 6S output enables easy computation of the Ångström exponent $\alpha_{\lambda_1,\lambda_2}$, as,

$$\alpha_{\lambda_1,\lambda_2} = -\frac{[\ln(\tau_{\lambda_1}) - \ln(\tau_{\lambda_2})]}{[\ln(\lambda_1) - \ln(\lambda_2)]}, \tag{3}$$

defined between the wavelength pair λ_1, λ_2. This depends on whether the low-AOD or high-AOD aerosol models are being used, and is a function of f_f. In the SeaWiFS aerosol product, this is calculated as $\alpha_{440,870}$, as this is a commonly used wavelength pair for aerosol studies. From this point all references to α indicate $\alpha_{440,870}$. The extreme values of α (approximately -0.1 for $f_\mathrm{f} = 0$, and 2 for $f_\mathrm{f} = 1$, calculated with Mie theory) are similar for both sets of aerosol models, although they have different nonlinear relationships between f_f and α.

2.3.1. Pure Maritime Model

[21] The microphysical model for pure (unpolluted) marine aerosol is presented by *Sayer et al.* [2012], and a summary of relevant details is provided here. This model was obtained from analysis of retrieved aerosol size distributions from eleven island Aerosol Robotic Network (AERONET) sites spread throughout global oceans [*Holben et al.*, 1998; *Dubovik and King*, 2000], considering only those retrievals interpreted as representing marine aerosol. Size distribution parameters showed a high consistency between sites. A recommended model with $r_{\mathrm{v,f}} = 0.157$ μm, $r_{\mathrm{v,c}} = 2.58$ μm, $\sigma_\mathrm{f} = 0.50$, $\sigma_\mathrm{c} = 0.72$, fine mode refractive index $m = 1.415 - 0.002i$ and coarse mode $m = 1.363 - 3 \times 10^{-9}i$ was found to reconstruct the AERONET AODs with a precision of 0.01–0.02, similar to that of the AERONET measurements themselves [*Holben et al.*, 1998; *Eck et al.*, 1999], when provided with $C_{\mathrm{v,f}}$ and $C_{\mathrm{v,c}}$ for each individual case. The single scatter albedo (SSA) is approximately 0.98 for the SeaWiFS wavelengths used.

2.3.2. Pollution and Dust-Influenced Models

[22] AERONET Level 2.0 (cloud-screened and quality-assured [*Smirnov et al.*, 2000]) Version 2 size distribution inversions from thirteen coastal sites with a significant non-marine contribution to their aerosol (listed in Table 1) were examined to construct microphysical models for high aerosol particle loadings. Only inversions where $\tau_{550} \geq 0.4$ with a successful refractive index retrieval were considered, to ensure the dominance of the AOD by the non-maritime component. Note that AERONET provides only a single refractive index for the model as a whole, not for constituent modes. As in work by *Sayer et al.* [2012], typical size distribution parameters were obtained for these sites from a bimodal lognormal distribution fit to the median value of $dV(r)/d\ln(r)$ for each bin from all of the qualifying size distributions at that site. These median distributions are presented in Figure 2.

[23] The sites fall into two distinct categories split by f_f, and within each of these categories, size distribution parameters

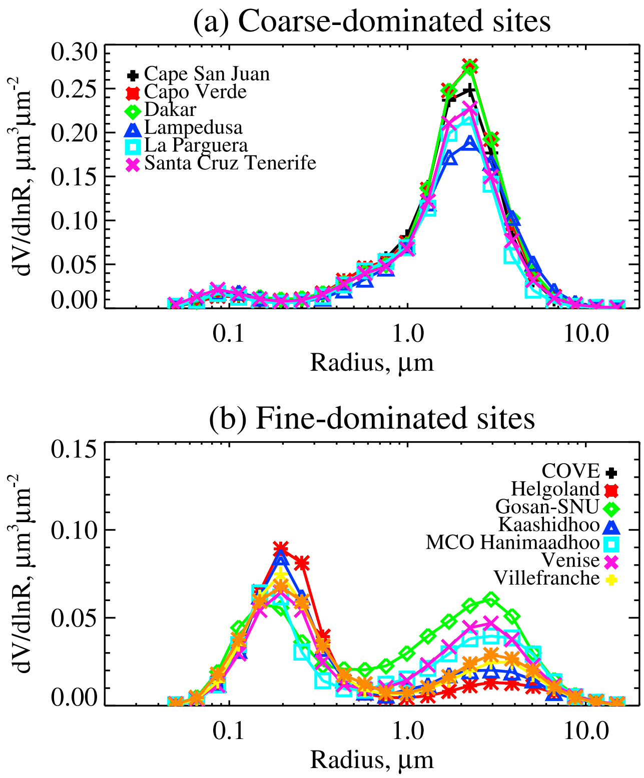

Figure 2. Averaged aerosol volume size distributions for the AERONET sites in Table 1, for high aerosol loadings, as described in the text. Plots are split to show separately sites where contributions from (a) the coarse mode and (b) the fine mode dominate the midvisible AOD.

(and refractive index) are similar, with much of the variability resulting from differences in aerosol volume (i.e. the size, rather than peak location or broadness, of the aerosol size distribution). The SOAR LUT uses the averages of the size distribution parameters for the six coarse-dominated sites ($r_{v,f} = 0.11$ μm, $r_{v,c} = 2.04$ μm, $\sigma_f = 0.43$, $\sigma_c = 0.49$) where $f_f \leq 0.25$, and the average of the seven fine-dominated sites ($r_{v,f} = 0.19$ μm, $r_{v,c} = 2.75$ μm, $\sigma_f = 0.44$, $\sigma_c = 0.65$) where $f_f > 0.25$. Modal radii and spreads were not observed to strongly depend on AOD, suggesting the same parameter combinations can be used for all elevated aerosol loadings. AERONET refractive indices are not calculated at wavelengths corresponding exactly to the SeaWiFS bands. Therefore, based on the average of the values retrieved by AERONET for the visible bands, $m = 1.43 - 0.0075i$ is used for both modes of the fine-dominated model and $m = 1.47 - 0.002i$ for both modes of the coarse-dominated model. Dependent on wavelength and f_f, the resulting SSA varies between approximately 0.88 and 0.96 for these models, respectively.

2.4. Response of ρ_{TOA} to AOD and f_f

[24] Figure 3 shows ρ_{TOA} as a function of τ_{550} and f_f for a typical tropical viewing geometry, corresponding to a high Sun and pixel near the center of the SeaWiFS swath. Generally, for a given wavelength, ρ_{TOA} increases with τ_{550} over the range plotted, while f_f influences the spectral shape of ρ_{TOA}. At high AODs the curves for $f_f = 0$ or 0.2 differ from the others in some situations; this is due to the different aerosol microphysical models used in the retrieval in these regimes.

[25] The near-infrared bands exhibit a drop in ρ_{TOA} as f_f increases, while for the other bands responses vary. At low AODs there is little change of ρ_{TOA} with f_f. This represents the ambiguous nature of size-related information from such

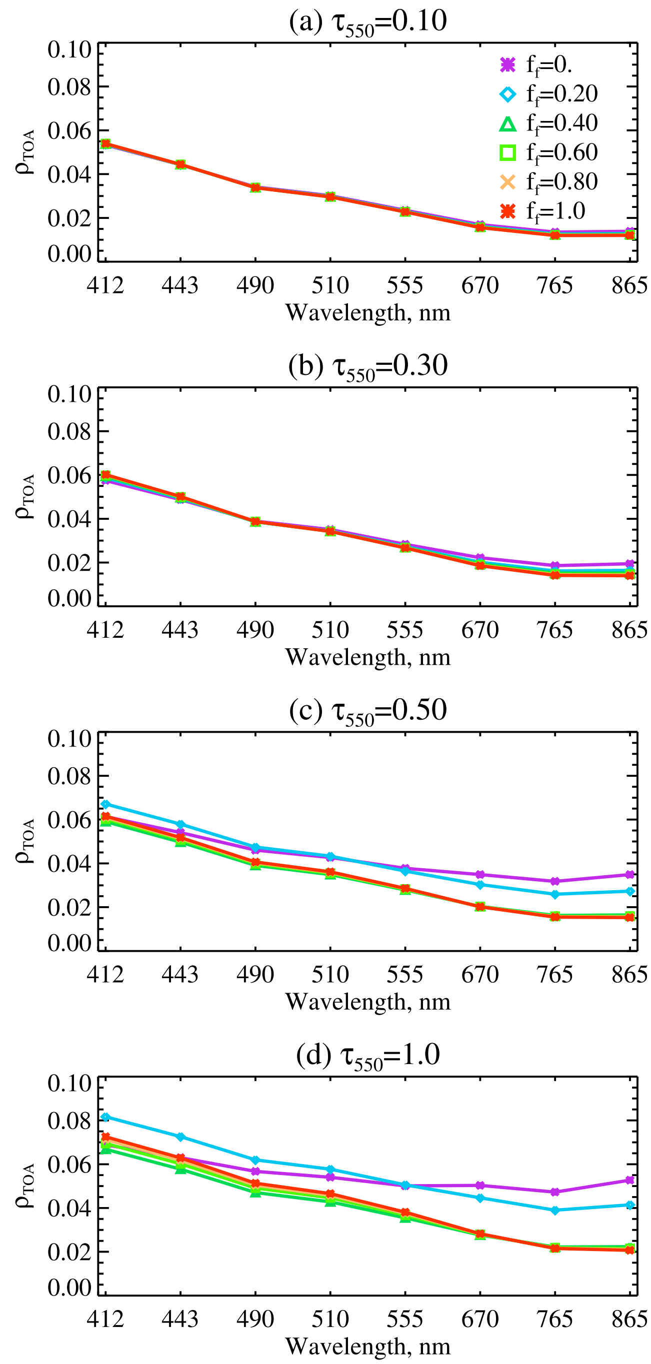

Figure 3. Response of spectral ρ_{TOA} to changes in τ_{550} and f_f, for all SeaWiFS bands (indicated along the x-axis). Plots show data for τ_{550} of (a) 0.1, (b) 0.3, (c) 0.5, and (d) 1. In all cases, the geometric conditions are $\theta_s = 8°$, $\theta_v = 22°$, and $\phi_r = 144°$, the wind speed is 6 ms^{-1}, and $chl = 0.2$ mg m^{-3}, all corresponding to typical values.

sensors for low aerosol particle loadings, and as such f_f is not expected to be quantitatively useful in these cases, as any signal may be dominated by calibration and forward model error [see also *Tanré et al.*, 1996]. Because of the size-parameter-dependence of Mie scattering, coarse mode scattering contributes comparatively more to aerosol extinction in the near-infrared, thus reconciling the decrease in ρ_{TOA} at 865 nm with increasing f_f (i.e. decreasing f_c). The availability of additional bands at longer wavelengths (e.g. 1.6 μm) would improve upon retrieval of f_f [*Tanré et al.*, 1996].

[26] At $\tau_{550} \leq 0.3$, the relative change of ρ_{TOA} with f_f is similar across the spectral range investigated. At higher AOD, the response is often stronger in the bands shorter than 510 nm. However, wavelengths shorter than 510 nm show increasingly strong dependence on *chl* (not shown). The 765 nm band behaves similarly to 670 nm and 865 nm bands, and is normally slightly darker than these bands as it overlaps with a strong oxygen absorption feature.

2.5. Sensitivity to FM Assumptions

[27] The effects of some assumptions built into LUT creation have been assessed with additional simulations using the 6S code. General tendencies are presented here, although exact results are dependent on the specific surface and atmospheric conditions. In particular, the impact of radiometric and aerosol microphysical errors tends to become more extreme for high AODs (around $\tau_{550} > 0.5$). Overall, f_f was found to be more susceptible than τ_{550} to FM errors [see also *Wagner and Silva*, 2008]. This highlights again the uncertainties involved in retrievals of size-related aerosol parameters, and requirement for aerosol microphysical models to be appropriate for this parameter to be useful. As τ_{550} is the primary quantity of interest, the discussion focusses on this parameter.

[28] First, an absolute radiometric uncertainty of 3% causes an uncertainty $\sim$0.01 in τ_{550}; effects on f_f are larger and more variable, dependent on geometry, the AOD, and the degree of spectral correlation between radiometric errors. The linear LUT interpolation used in the retrieval was found to introduce errors generally less than 3% in ρ_{TOA}, suggesting this is a minor contribution to the error budget. Similarly, a 20% change in total column ozone has a negligible effect on ρ_{TOA} at the wavelengths used.

[29] Changes in assumed surface reflectance (e.g. decreased ρ_{TOA} at 510 nm from increased absorption by colored dissolved matter, or increased ρ_{TOA} at all wavelengths from enhanced particle backscattering in turbid waters) affect the retrieval in proportion to their effect on ρ_{TOA}. For example, a doubling of ρ_{TOA} as a result of water turbidity causes a positive error in retrieved τ_{550} around 0.25. These are therefore likely to be performance-limiting factors in turbid waters. However, varying *chl* in the range $0.01 \leq chl \leq 10$ mgm^{-3} affects retrieved τ_{550} by 0.01 or less, and f_f by 0.05 or less. This is because underlight decreases rapidly with increasing wavelength, and the 510 nm channel occupies a spectral 'hinge point' at which the water-leaving radiance is less variable compared to other wavelengths. In moderate and strong sunglint, errors in assumed wind speed of 2 ms^{-1} lead to errors of opposite sign in τ_{550} of 0.05 or more, and overwhelm the signal for f_f. However, away from glint, wind speed errors of this size have negligible impact on the retrieval for $ws < 6$ ms^{-1}, and errors in τ_{550} up to 0.025 for $6 \leq ws \leq 15$ ms^{-1}.

[30] Altering aerosol particle modal radii by 10% individually affects ρ_{TOA} by 1%–4%, translating into an error in τ_{550} around 0.01 for each. Altering modal spreads by 10% has an effect of typically 1% or less in ρ_{TOA}, i.e. a minor impact on the retrieval. Changes in the midvisible SSA have, to a first order, an effect on retrieved τ_{550} commensurate with the error in SSA (i.e. a relative underestimate of SSA causes an relative overestimate of τ_{550} by a similar amount). As SSA is typically close to 1, this is a negligible source of absolute uncertainty at low AOD, but important for high AOD.

[31] The assumption of spherical particles may lead to additional uncertainties when the AOD is dominated by dust. An alternative in such cases is to assume mixtures of spheroids of various aspect ratios, or more complicated shapes, and use T-Matrix theory or other methods instead of Mie theory [e.g., *Mishchenko et al.*, 1996; *Kalashnikova et al.*, 2005; *Dubovik et al.*, 2006]. However, decisions must then be made as to the appropriate shape distribution(s) to use. The effects of nonspherical dust microphysical models have not been assessed here; however, validation efforts in Section 3 suggest that retrievals of AOD in such cases remain high quality.

[32] Combining uncertainties in radiometry, four aerosol microphysical model parameters, and moderate wind speeds, and assuming the perturbations tested are representative and occur independently of each other, a first-order theoretical estimate for the uncertainty in τ_{550} for low to moderate AOD under typical conditions is $\sim$0.03.

2.6. Postprocessing and Retrieval Quality Flags

[33] In the postprocessing stage, retrieved τ_{550} and f_f and other relevant information (such as Sun-sensor geometry) are aggregated at 3 $\times$ 3 pixel resolution (known as 'cell' resolution, around 13.5 km $\times$ 13.5 km at the center of the swath), and written to the Level 2 file (retrieval output from a single orbit). This contains the cell-averaged τ_{550} and f_f, which are then used to calculate α and the AOD referenced to the three SeaWiFS bands used in the retrieval (510 nm, 670 nm, 865 nm). As the spatial variability of AOD on this scale is generally smooth and small [*Anderson et al.*, 2003], averaging to cell resolution decreases noise on the retrieved values. The statistics of the retrievals within each cell are used to assign a quality assurance (QA) flag, which indicates the level of confidence in the cell-averaged retrieved AOD. The QA flag takes values from 0 to 3, where 0 indicates no data and 1–3 increasing confidence in the retrievals. Over the ocean, it is recommended for quantitative purposes to only use cells with QA $\geq$ 2 (discussed in Section 3).

[34] The rationale behind QA flagging is largely based on the principle that the most frequent and largest causes for poor-quality retrievals are related to cloud contamination, and cases of poor surface modeling (Section 2.5). Initially, all cells containing at least one valid retrieval are assigned a QA flag of 1. For each cell, the number of pixels which either lack ocean retrievals, or have a difference in τ_{550} of the greater of 50% or 0.5 in comparison with the central pixel of the cell, are counted. Steep gradients or missing retrievals are signs of cloud-contamination, proximity to clouds, or proximity to coast. If fewer than six pixels meet these criteria (i.e. at least 4 out of 9 pixels are present and the cell is reasonably homogeneous), then the QA flag is raised

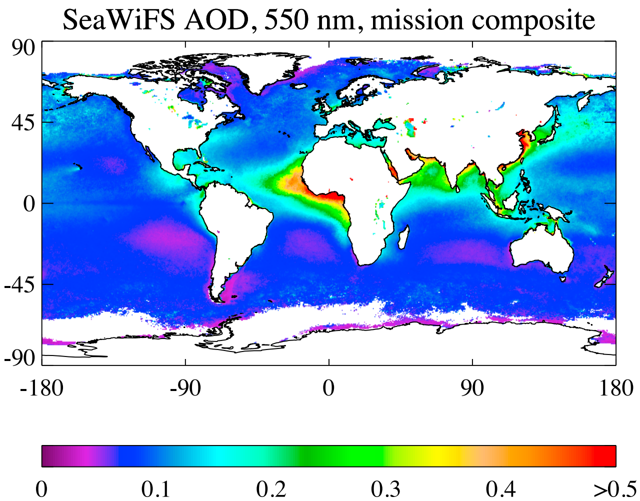

Figure 4. Whole-mission (1997–2010) averaged SeaWiFS AOD at 550 nm at 0.5° resolution. Created by averaging monthly mean AODs, and shown only for those grid cells with at least 10 months contributing to the average.

to 2. If fewer than three pixels meet these criteria (i.e. at least 7 out of 9 pixels are present and lack steep gradients), the QA flag is raised to 3.

[35] Next, the glint reflectance of the ocean surface (ρ_{gl}) is calculated at 550 nm using the wind speed and geometry [*Cox and Munk*, 1954a, 1954b]; if $log_{10}(\rho_{gl}) > -2.5$, the cell is marked as glint-contaminated, and the QA flag is set to 1. The threshold was determined empirically by examining statistics of retrieved quantities as a function of glint strength, and results in approximately 15% of retrievals being set to QA = 1. These retrievals are located in the tropics and their exact position varies seasonally.

[36] One additional piece of information available is the quality of the fit (sum of squared residuals). If the cell-averaged absolute total square residual on fit ρ_{TOA} is 0.01 or more, the QA flag is also set to 1. Typical residuals for well-fit retrievals are generally a tenth to a half of this value. In some turbid waters an acceptable quality of fit was found, although the retrieved AODs were unphysically high, when examined in the context of nearby cells and visible imagery. This occurs because the surface reflectance is significantly brighter than assumed by the FM (Section 2.5), and is an issue known to be common to many satellite data sets [e.g., *Kahn et al.*, 2010]. Therefore cells where $\tau_{550} \geq 0.9$ but the Lambertian-equivalent reflectivity (LER) [*Dave*, 1976] at 865 nm is less than 0.04 are also set to QA = 1. These thresholds were based on manual examination of cases of cloud, sea ice contamination, and highly turbid waters. Testing in other regions revealed that the number of high-AOD events (e.g. dust storms or smoke plumes) removed by these tests are negligible, and they are therefore unlikely to introduce a sampling bias against these events in the SOAR data.

[37] When the AOD is low, there is not much information in the measurements relating to particle size (Figure 3), and f_f and so α become highly uncertain [*Wagner and Silva*, 2008]. Therefore quantitative use of f_f and α is not recommended for $\tau_{550} < 0.3$, and a separate QA flag is provided for them. This is set equal to the AOD QA flag for $\tau_{550} \geq 0.3$, and 1 otherwise.

[38] Using these criteria, approximately 25% of AOD retrievals have QA = 2, with small spatial variability. QA = 1 accounts for ~35% of retrievals, and is more common in regions of high cloudiness (e.g. the storm tracks), tropical Sun-glint zones, and most inland waters, accounting for ~50% of retrievals in the first two of these situations and 80% or more in the third. The remaining retrievals assigned QA = 3 (~40%) are most concentrated in oceanic regions of low cloudiness (e.g. far from marine stratocumulus decks or the storm tracks). A composite image of QA ≥ 2 retrievals, created from the whole time series, is shown in Figure 4, revealing the expected [e.g., *Smirnov et al.*, 2011] global variability of AOD over oceans, largely free from obvious artifacts.

3. Validation With AERONET Data

3.1. AERONET Coastal and Island Sites

[39] Although some theoretical considerations for retrieval performance are given in Section 2.5, validation against independent data sources is a necessary step in evaluation of the data. For this purpose, retrieved τ_{550}, τ_{870}, and α, have been compared to direct-sun AERONET measurements. Performance at intermediate wavelengths such as 670 nm can be inferred reasonably from these bounding wavelengths. A total of 49 sites, limited to those that have a reasonable data record (generally one or more years of level 2.0 data), are within approximately 1 km of the coast, and are at low elevations, were used. As noted in various other studies, the AERONET and satellite data differ fundamentally in that AERONET samples one location at high temporal frequency, while satellites provide data with a larger spatial footprint, typically over a wide swath, but with poorer temporal resolution [*Ichoku et al.*, 2002; *Kahn et al.*, 2010; *Hyer et al.*, 2011]. Therefore, to optimize the representativeness of the comparison, AERONET AOD data are averaged over a 30 minute temporal window centered on the time of the SeaWiFS overpass, while SeaWiFS retrievals are averaged over a circle of 25 km radius centered on the AERONET site.

[40] AERONET quantities are denoted with a subscripted A (e.g. $\tau_{A,\lambda}$). Because of the mismatch between SeaWiFS and AERONET wavelengths, $\tau_{A,550}$ is calculated from equation (3), using α_A together with the spectrally closest AERONET AOD (either 440 nm or 500 nm). Manual inspection of the AERONET data suggests that, as the AERONET AOD is typically spectrally smooth, the uncertainty introduced by this interpolation is negligible. The SeaWiFS 865 nm band is close to the AERONET 870 nm band, so these quantities are compared directly (referred to as '870 nm', so τ_{870}, for ease). Similarly, the 5 nm difference in wavelengths has a negligible effect. Both SeaWiFS and AERONET α used in this comparison are defined between 440 nm and 870 nm.

[41] Considering only QA = 3 retrievals there are 8,911 matches. Pearson's linear correlation coefficient R is 0.86 at 550 nm and 0.90 at 870 nm. Correlation for α is poorer (0.50). However, when only points where $\tau_{A,550} \geq 0.3$ are considered, this increases to 0.78. Scatter density plots are presented in Figure 5. The majority of points are for $\tau_A \leq 0.2$

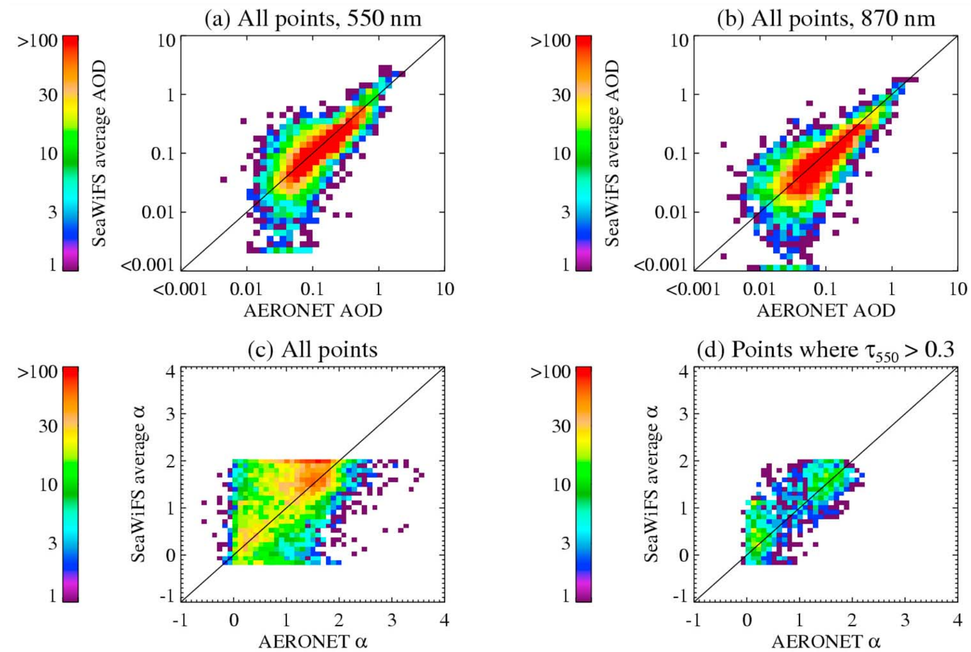

Figure 5. Scatter density plots for colocated AERONET and SeaWiFS data (for QA = 3). AOD at (a) 550 nm and (b) 870 nm. Ångström exponent: (c) separately for all points and (d) only those points where the AERONET AOD at 550 nm is at least 0.3.

(at both wavelengths), and there is a slight tendency for the algorithm to underestimate the AOD (median SeaWiFS-AERONET bias of −0.013 at 550 nm, and −0.011 at 870 nm). As well as retrieval and calibration error in both data sets, part of the scatter can be related to sampling and sub-pixel heterogeneity. *Hyer et al.* [2011] and *Kahn et al.* [2011] discuss implications of related satellite sampling issues when comparing to AERONET data.

[42] The scatter about the offset between the two data sets is described by the scaled median absolute deviation, denoted σ_{med}, where

$$\sigma_{\mathrm{med}}(x) = \beta(\widetilde{x - \tilde{x}}), \qquad (4)$$

where ∼ indicates a median quantity, x is the SeaWiFS-AERONET difference for one matched pair of data, and β is a scaling factor. If the underlying distribution is Gaussian, then σ_{med} is equivalent to the standard deviation for $\beta = 1.4826$, which is assumed here. Thus σ_{med} is an outlier-resistant measure of the scatter about this bias. Here, $\sigma_{\mathrm{med}} = 0.045$ at 550 nm and 0.033 at 870 nm, while the respective standard deviations of the difference are 0.088 and 0.056. The difference between these two metrics indicates that there are some outliers, although Figure 5 shows that the majority of points cluster closely around the 1:1 line.

[43] The SeaWiFS-AERONET offset is presented as a function of τ_{A} in Figure 6. SeaWiFS has a positive relative AOD offset in the cleanest AERONET cases (by an average

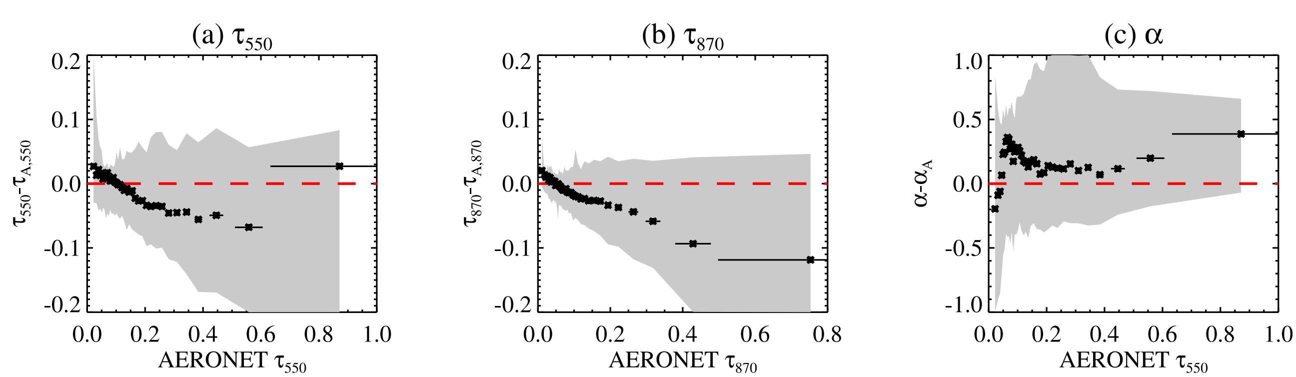

Figure 6. Mean SeaWiFS-AERONET bias in retrieved (a) τ_{550}, (b) τ_{870}, and (c) α as a function of AERONET AOD. Data are binned in order of ascending τ_{A}, with a bin size of 250 matchups. Horizontal error bars indicate the standard deviations on the bin-averaged AERONET AOD; the shaded grey area shows one standard deviation around the mean SeaWiFS-AERONET bias. Only points where QA = 3 are included.

of 0.03 or less), and a relative negative bias around −0.05 for AODs between approximately 0.2 and 0.4. The majority of the samples are for low-AOD cases where bias is small. For the highest AERONET AODs, the SeaWiFS 550 nm AOD relative bias is closer to zero. Although these differences are within the expected uncertainty, the results suggest a potential underestimate of surface reflectance, or residual cloud contamination in the SeaWiFS data, for some very clean cases. Cirrus contamination in the AERONET data [e.g., *Huang et al.*, 2011], and the choice of the LUT switchover point between marine and non-marine aerosol model, could contribute to the relative low bias for moderate AODs. SeaWiFS τ_{870} exhibits an offset that is initially small and positive (0.01–0.02) and becomes linearly more negative with increasing AERONET AOD, although again for the majority of points the average bias is small. There is a general tendency for SeaWiFS to overestimate α, which suggests insufficient spectral variability in the assumed surface reflectance (so the retrieval increases the spectral variability of AOD to give the best match to ρ_{TOA}).

[44] If retrievals where QA = 2 are also included, the comparison sample size increases significantly to 12,313. The correlation coefficient remains 0.86 at 550 nm and decreases slightly to 0.88 at 870 nm; σ_{med} and the standard deviation increase by around 10%, to 0.051 and 0.036 for σ_{med}, and 0.092 and 0.063 for the standard deviation, at 550 nm and 870 nm respectively. The offsets become less negative; −0.004 at 550 nm and −0.005 at 870 nm. This shows that adding QA = 2 retrievals increases coverage, but does not significantly degrade performance. These QA = 2 data are thus suitable for general use, as well as QA = 3.

[45] If QA = 1 data are included, the sample size further increases to 14,750. Correlation coefficients decrease (0.84 and 0.86), the relative offsets become more positive (−0.001 and −0.004), σ_{med} increases (0.054 and 0.039), as does the standard deviation (0.097 and 0.068), where all statistics in parentheses are for 550 nm and 870 nm respectively. In some circumstances, QA = 1 data may also be useful. However, there is a clear decrease in retrieval quality as the assigned QA flag decreases. The true difference in quality between the quality flags may to an extent be masked here, as a primary reason for a low quality flag is linked with an increased possibility of cloud contamination, while the matchups here are by nature effectively doubly cloud-screened (i.e. the chance for cloud contamination for the subset of AERONET matchups is probably lower than for any random subset of retrievals).

[46] Validation results have also been examined subset by Sun/sensor geometry, and by wind speed. No general trends with respect to geometry were found. A tendency for a small negative bias in AOD with increasing wind speed, becoming more negative by about 0.03 over the range of 0–10 ms^{-1}, was found. This suggests that the sea surface reflectance model in 6S may not capture the spectral wind speed-dependence of surface reflectance accurately, by overestimating the increase of surface reflectance (due to whitecaps) with wind speed. However, this is only a small contribution to the total retrieval error. Within individual geometric or wind speed bins, the distribution of $\tau - \tau_A$ is approximately Gaussian.

3.2. Estimation of Expected Error

[47] If uncertainties in the measurements, FM, and ancillary data are well-characterized then techniques such as optimal estimation enable calculation of the retrieval random error on a pixel-by-pixel basis, although these estimates are contingent upon the quality of assumed input uncertainties [*Rodgers*, 2000]. As this is not the case here, uncertainties are estimated through the comparison with AERONET data, which can be considered a reasonable comparative baseline (uncertainty of order 0.01–0.02 [*Holben et al.*, 1998; *Eck et al.*, 1999]). The AOD retrieval error $\epsilon(\lambda)$ is then defined as the difference between SOAR and AERONET AODs, i.e. $\tau_\lambda - \tau_{A,\lambda}$. Limiting factors on the retrieval's performance at low AODs are expected to be improper characterization of surface reflectance, and at high AODs errors in assumed aerosol radiative properties, and so the general trend of the absolute error ($|\epsilon|$) is expected to be of the form $a + b\tau_A$, such that there is both some absolute minimum error and some AOD-dependent contribution (e.g., Section 2.5) [*Levy et al.*, 2010; *Kahn et al.*, 2011]. The aim is then to estimate a, b to provide a confidence interval for the retrieved AOD, such that one standard deviation (68%) of retrievals have $|\epsilon| \le a + b\tau_A$, and two standard deviations (95%) have $|\epsilon| \le 2 \times (a + b\tau_A)$. The function $a + b\tau_A$ will from here be known as the 'expected error' (EE). Although this is not something which can be assessed on the basis of individual retrievals, the goal is to estimate the typical absolute uncertainty in the AOD retrieval.

[48] Testing of a selection of parameters a and b reveals that appropriate values (i.e. approximately 68% of data with this error or better, and 95% twice this or better) for the EE are around $0.03 + 0.15\tau_{A,550}$ and $0.03 + 0.10\tau_{A,870}$, which are met by 68% of matchups overall at 550 nm, and 71% at 870 nm. If QA = 2 are also permitted, this decreases to 67% at 550 nm and 69% at 870 nm, showing this EE is still appropriate. When QA = 1 retrievals are included, these values decrease to 65% at 550 nm and 67% at 870 nm. Performance was also examined on a site-by-site basis; at most sites, between 50% and 80% of retrievals fall within the desired EE, with little dependence on region. Sites with frequent dust episodes (Capo Verde, Dakar) show increased scatter at moderate and high AODs, perhaps due to errors in the dust phase function used in the retrieval, or aerosol heterogeneity. Altering the averaging distance for SeaWiFS data, the averaging time for AERONET, or picking the nearest rather than average SeaWiFS retrieval has been tested and found not to significantly affect the statistics of the comparison (with correlation coefficients varying by 0.01–0.05, and σ_{med} or standard deviation changing by around 10%). This EE is similar to the sensitivity study results; additional contributions to the EE not considered in Section 2.5 include factors such as the 6S radiometric accuracy, cloud-contamination, sampling issues, and errors in the AERONET data.

3.3. Maritime Aerosol Network Cruises

[49] The Maritime Aerosol Network (MAN) component of AERONET consists of spectral AOD measurements made on board ocean cruises [*Smirnov et al.*, 2009, 2011]. These data are typically collected with hand-held Microtops II Sun photometers, which enable determination of AOD with an accuracy of approximately 0.02 [*Knobelspiesse et al.*, 2004]. Taken together, AERONET and MAN allow evaluation of AOD over a wider range of marine conditions. Here, the 'series average' (measurements acquired with a gap of no more than two minutes between each) Level 2.0 product is

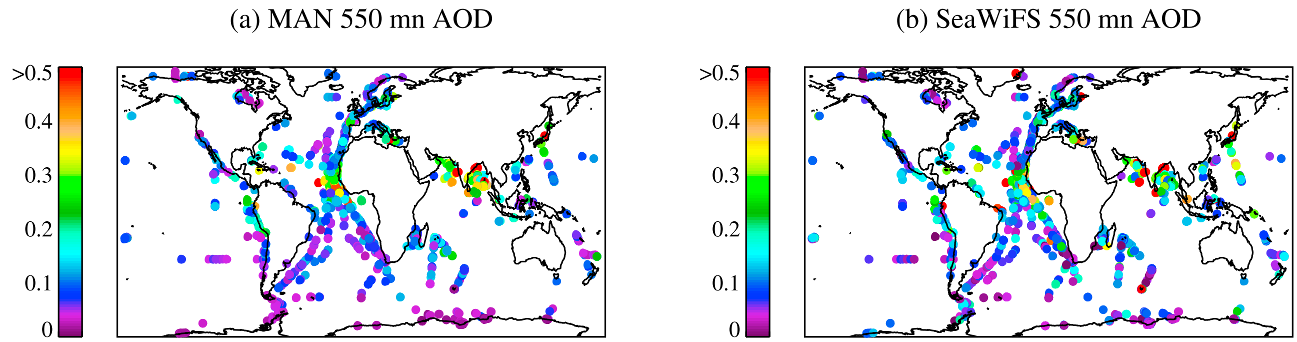

Figure 7. Map of AOD at 550 nm (a) from MAN observations and (b) retrieved by SeaWiFS, with loose criteria on colocations (up to 3 hours in time, and 100 km in space) and quality flags (any SeaWiFS QA allowed).

compared to the nearest SeaWiFS retrieval during the period of collection. In contrast to the AERONET ground sites, here the nearest SeaWiFS cell is used because the ship is also moving (albeit at a much slower speed than the satellite), although the statistics of the comparison are similar if an area-averaged SeaWiFS AOD is used instead.

[50] The number of comparisons possible is sensitive to the permitted maximum time between the MAN measurements and SeaWiFS overpass, the maximum permitted distance between the ship and the nearest SeaWiFS retrieval, and the minimum permitted SeaWiFS retrieval QA value. Figure 7 shows the comparison of 550 nm AOD for a loose set of colocation criteria (any SeaWiFS QA, time difference 3 hours or less, distance difference 100 km or less); this leaves 3,426 matches between the two data sets (some points in Figure 7 lie on top of each other). Even with this set of colocation criteria, there is a high degree of agreement between the data sets, with SeaWiFS capturing the regional variability of AOD well. Statistics for this comparison and a stricter set of colocation criteria, to ensure a more direct matchup and include only high-quality retrievals (QA = 3, time difference 1 hour or less, distance difference 10 km or less, leaving only 280 matches), are given in Table 2. Similar to the comparison with AERONET coastal and island sites, a high degree of correlation with a slight low bias in AOD is found. For the tighter colocation criteria, 78% of retrievals fall within the expected uncertainty at 550 nm (67% at 870 nm), indicating performance is also good for open-ocean retrievals (slightly better at 550 nm, and slightly worse at 870 nm). If the 'tight' subset is expanded to allow points with QA = 2, the number of matches increases, but the quality of the comparison decreases (although is still high). As with the AERONET sites, some residual cloud contamination may be present in the MAN data (notably under heavy aerosol loading, where visual identification of clouds may be more difficult), although in these cases it is possible that this cirrus may also be undetected by SeaWiFS.

4. Comparison With Other Satellite Data

4.1. OBPG SeaWiFS Product

[51] The SeaWiFS Ocean Biology Processing Group (OBPG) data processing chain involves an atmospheric correction, described by *Ahmad et al.* [2010], required for the subsequent retrieval of chlorophyll concentration and other properties. Factors including differences in cloud masks and retrieval resolution mean that a direct comparison between the SOAR algorithm presented here and SeaWiFS OBPG algorithm on a pixel-by-pixel basis is not possible. At a minimum, aggregation to a common grid would be necessary. The OBPG algorithm provides τ_{865}, used for atmospheric correction of the visible ocean-color bands. Stringent tests are applied to exclude those pixels potentially influenced by clouds or high AODs, which could lead to errors in the retrieved water-leaving radiance, i.e. it is not explicitly designed to provide an aerosol climatology in the same way as SOAR or other data sets. For these reasons, the comparison with OBPG SeaWiFS data is performed in a different way from those presented in the next Section.

[52] Figure 8 shows τ_{865} from 11 March 2006 over the tropical Atlantic and Indian Ocean. Here, the SOAR retrieval is shown for cells where QA ≥ 2, and the OPBG algorithm where none of the default Level 2 processing warning flags (sun-glint, algorithm failure, cloudiness, and other checks) are set. This provides an example where pixels with high aerosol loadings, such as Saharan dust outflow into the tropical

Table 2. Statistics of Comparison Between SeaWiFS and MAN AODs at 550 nm and 870 nm, for Tight and Loose Colocation Criteria[a]

Criteria	Number of Matches	AOD at 550 nm R	Bias	σ_{med}	$p(\|\epsilon\| \le EE)$	AOD at 870 nm R	Bias	σ_{med}	$p(\|\epsilon\| \le EE)$
Tight, QA = 3	279	0.89	−0.022	0.031	0.78	0.89	−0.021	0.026	0.67
Tight, QA ≥ 2	411	0.87	−0.017	0.037	0.74	0.85	−0.019	0.029	0.69
Loose	3,426	0.79	−0.0005	0.050	0.63	0.74	−0.008	0.036	0.66

[a]Tight denotes time difference ≤1 hour, distance difference ≤10 km; either QA ≥ 2 or QA = 3. Loose denotes any SeaWiFS QA, time difference ≤3 hours, distance difference ≤100 km. R is Pearson's linear correlation coefficient. The bias is the median offset between the data sets, defined such that positive values indicate SeaWiFS AODs are larger. The scaled median absolute deviation of the difference between the two data sets is denoted σ_{med}. Finally, p is the proportion of retrievals with absolute error $|\epsilon|$ smaller than the expected error (EE), $0.03 + 0.15\tau_{550}$ at 550 nm, or $0.03 + 0.1\tau_{870}$ at 870 nm.

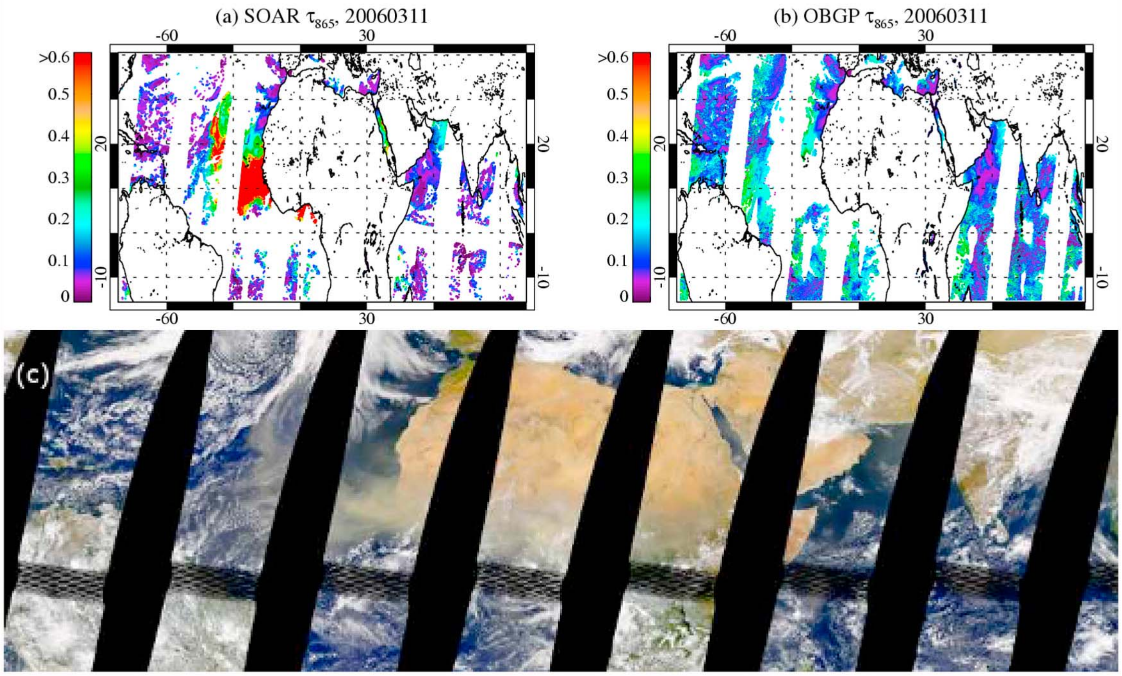

Figure 8. SeaWiFS data over the tropical Atlantic and Indian Oceans (15° S-40° N, 80° W-100° E) from 11 March 2006. Plots show AOD at 865 nm from (a) the SOAR SeaWiFS algorithm, and (b) from the OBPG algorithm. (c) True-color SeaWiFS composite image. Stripes near the Equator are where the SeaWiFS tilt reverses.

Atlantic Ocean are often masked out or retrieved with lower AODs by the OBPG algorithm. The SOAR QA flags mask out more data as cloud-contaminated than the OBPG algorithm. In low-AOD regions, spatial patterns are similar, although the absolute values frequently differ by 0.02–0.05, particularly near cloud edges.

[53] Using the database of AERONET matchups (for SOAR QA ≥ 2, a 30 minute AERONET average, and 25 km SeaWiFS average), OBPG τ_{865} retrievals have also been extracted and averaged, using the same averaging distance, and default checks on processing warning flags in the OBPG data. This leaves a total of 11,696 colocated data points with all three data sets present. The median SeaWiFS-AERONET offset is -0.003 for SOAR and 0.011 for OBPG. The absolute retrieval differences compared to AERONET are very similar for the two SeaWiFS data sets. The correlation between the SOAR and OBPG τ_{865} is 0.73; the mean (and median) relative SOAR-OBPG bias is -0.013, and the standard deviation (σ_{med}) about this bias 0.044 (0.029). The wind speed-dependent whitecap fraction used by the OBPG algorithm [*Stramska and Petelski*, 2003] is lower by between a factor of 2 and an order of magnitude than that used in 6S for typical wind speeds, meaning more of the TOA signal will be attributed to aerosol in the OBPG data, which will contribute to the difference between SOAR and OBPG at moderate or high wind speeds. Of the 49 AERONET sites, the SOAR algorithm has a smaller absolute bias at 27, and a larger absolute bias at 22. It is worth noting again that high AODs (e.g. dust at Capo Verde and Dakar) are missing from this subset of data, as the OBPG algorithm does not retrieve AOD in these conditions.

[54] The vicarious calibration gains applied to the SeaWiFS radiances depend on the OBPG atmospheric correction algorithm (although were not derived from the AERONET sites used here), and so include compensating errors when this atmospheric correction is incorrect [*Franz et al.*, 2007]. As the SOAR algorithm uses these calibration results, these compensating errors will tend to degrade SOAR performance. To test the possible effects of this, the SOAR algorithm was applied to the same set of AERONET matches without using the vicarious gains; the resulting differences in retrieval results were of order 0.01 in AOD and 0.1 in f_f, and the overall quality of the comparison with AERONET was very slightly degraded, i.e. the current vicarious calibration provides benefit, or at least no harm, to the SOAR algorithm.

4.2. Other Data Sets

[55] Comparison of the SOAR retrievals with those from other satellite data sets provides insight into the performance of the retrieval on a global scale. Agreement and patterns of difference between data sets can be examined in the context of their own strengths and weaknesses. Each data set samples at different times and resolutions, and therefore a direct matchup between any two is difficult or impossible. Sampling and aggregation decisions can influence the results of such comparisons significantly [*Levy et al.*, 2009; *Sayer et al.*, 2010b], and so in this study efforts are made to minimize the effects of spatiotemporal mismatch between the data on the comparison. For this reason, all the comparisons use daily aggregated data as a basis. The following aerosol data sets are considered.

1. Multiangle Imaging Spectroradiometer (MISR) AODs at 558 nm and 865 nm, from the Version 22 algorithm [*Martonchik et al.*, 1998, 2009; *Kahn et al.*, 2010].

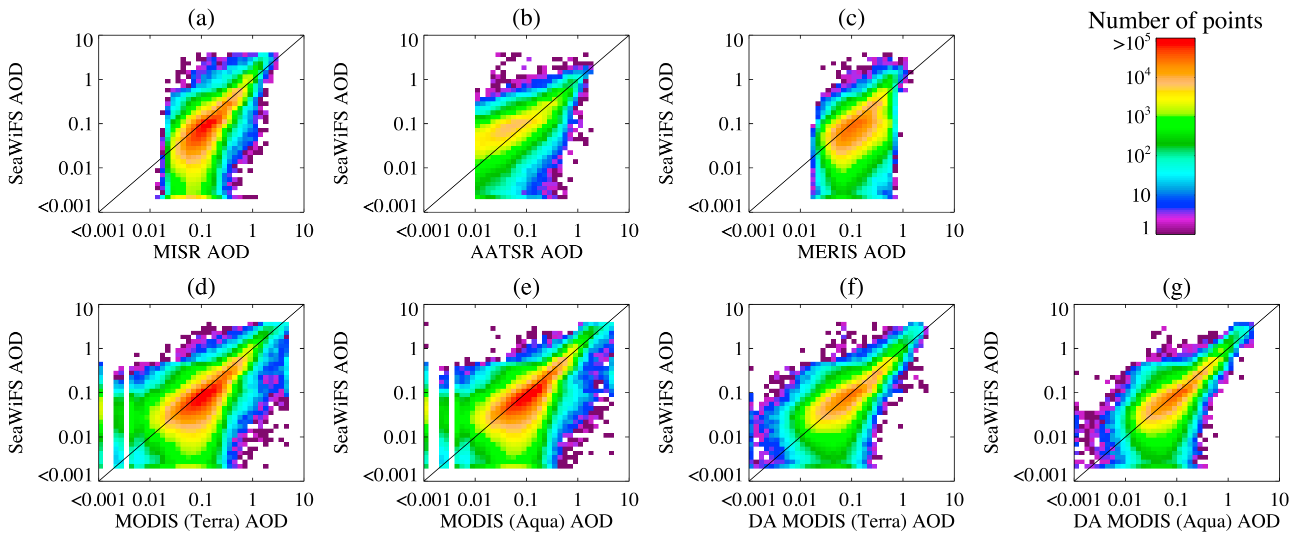

Figure 9. Scatter density plots between colocated daily averaged SeaWiFS τ_{550} and that from other data sets: (a) MISR, (b) AATSR, (c) MERIS, (d) MODIS (Terra), (e) MODIS (Aqua), (f) DA MODIS (Terra), and (g) DA MODIS (Aqua).

2. Advanced Along-Track Scanning Radiometer (AATSR) AODs at 550 nm and 870 nm, from the Oxford-Rutherford Appleton Laboratory (RAL) Aerosols and Clouds (ORAC) retrieval [*Thomas et al.*, 2009; *Sayer et al.*, 2010a].

3. MODIS AODs at 550 nm and 865 nm, from the most recent MODIS Science Team Collection 5.1 data set [*Remer et al.*, 2006, 2008]. The sensors aboard the Terra and Aqua satellites are considered separately (daytime Equatorial local solar crossing times approximately 10:30 am and 1:30 pm respectively, at the center of the swath).

4. The 'data-assimilation (DA) quality' MODIS AOD at 550 nm (hereafter DA MODIS), created by applying empirical bias corrections and additional cloud screening to MODIS Collection 5.1 data [*Zhang and Reid*, 2006; *Shi et al.*, 2011]. Terra and Aqua are again considered separately.

5. MEdium Resolution Imaging Spectrometer (MERIS) AODs at 550 nm and 870 nm, processed as part of the GlobAerosol project [*Antoine and Morel*, 1999; *Poulsen et al.*, 2009]. Daily composites of successful retrievals on a 10 km sinusoidal grid have been averaged to a 1° latitude and longitude grid.

[56] The period 2005–2007 is investigated, aside from AATSR (2006 and 2008) and DA MODIS (2006 and 2010), as the complete 2005–2007 period is not available for these data sets. All are at 1° horizontal resolution, except MISR, which is at 0.5°. Because the number of points where every sensor includes data on the same day is near-zero, colocations are performed between SeaWiFS and each other data set on an individual basis. To be considered for the comparison, grid cells in the daily products are only considered where both data sets contain at least 10 retrievals. The finer resolution of MISR means that this is reduced to 3 retrievals, this threshold being roughly equivalent given the different grid size.

[57] Scatter density histograms of the resulting matched data (at 550 nm) are shown in Figure 9, and statistics of these data are given in Table 3. These provide a general overview of the level of scatter and any global biases between the data sets. The scatterplots are very similar for MODIS (Terra and Aqua, both MODIS Science Team and DA MODIS) and MISR, all being higher than SeaWiFS for the low-AOD cases and lower for the highest-AOD cases. The strongest statistical agreement is with the DA MODIS data sets. However, it is not straightforward to say that this is solely due to the bias-correction procedures used to create the DA MODIS data, as around half of all points are also removed from the comparison by additional cloud screening in the DA MODIS product, including those points where both

Table 3. Statistics of Comparison Between Colocated SeaWiFS Daily Averaged AOD and That From Other Data Sets[a]

Data Set	Number of Grid Cells	τ_{550}			τ_{865}		
		R	Bias	σ_{med}	R	Bias	σ_{med}
MISR, version 22	2,173,079	0.84	−0.036	0.040	0.83	−0.025	0.031
AATSR, ORAC research	372,754	0.77	0.017	0.039	0.68	0.003	0.026
MODIS (Terra), Collection 5.1	3,118,321	0.80	−0.027	0.044	0.76	−0.028	0.038
MODIS (Aqua), Collection 5.1	3,162,926	0.82	−0.018	0.038	0.78	−0.021	0.033
DA MODIS (Terra)	907,069	0.87	−0.006	0.035	-	-	-
DA MODIS (Aqua)	944,380	0.90	−0.009	0.032	-	-	-
MERIS, GlobAerosol	1,182,703	0.55	−0.034	0.054	0.47	−0.026	0.050

[a]R is Pearson's linear correlation coefficient between the grid-box average values. The bias is the median bias between the daily average values, defined such that positive values indicate SeaWiFS AODs are larger. The scaled median absolute deviation of the difference between the two data sets is denoted σ_{med}.

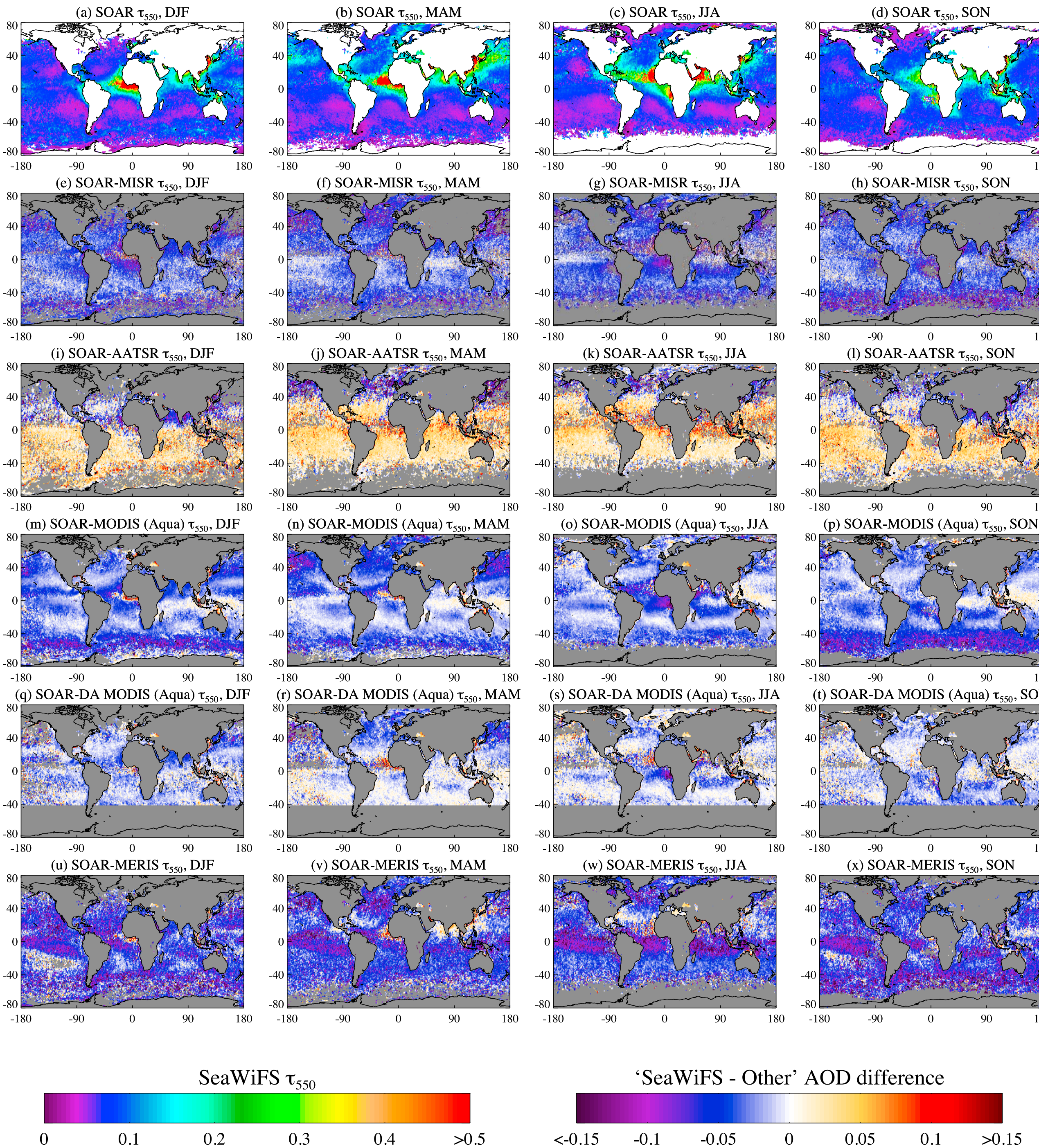

Figure 10. (a–d) SeaWiFS seasonal average over-ocean AOD at 550 nm at 1° resolution, from the mean of daily average AODs in which at least ten retrievals (QA $\geq$ 2) contributed to the daily average value, for the period 2005–2007. Also shown are seasonal mean difference between SeaWiFS and other AOD data sets, constructed from only those days of data where both data sets are well-sampled, as defined in the text: (e–h) MISR, (i–l) AATSR, (m–p) MODIS (Aqua), (q–t) DA MODIS (Aqua), and (u–x) MERIS. In the difference plots, grid cells without data are indicated in grey.

SeaWiFS and MODIS data are more likely to be prone to error. MODIS Terra exhibits a median high offset of 0.009 as compared to Aqua at 550 nm for the colocated subset of points (0.007 at 865 nm). The statistics are otherwise very similar, which is consistent with the results of *Remer et al.* [2008]. The differences between the sensors are largely removed in the DA MODIS product.

[58] *Kahn et al.* [2010] report that MISR yields a positive bias of order 0.025 at 550 nm over oceans as compared to AERONET. *Smirnov et al.* [2011] present similar results for MISR and MAN. If this offset is subtracted from the

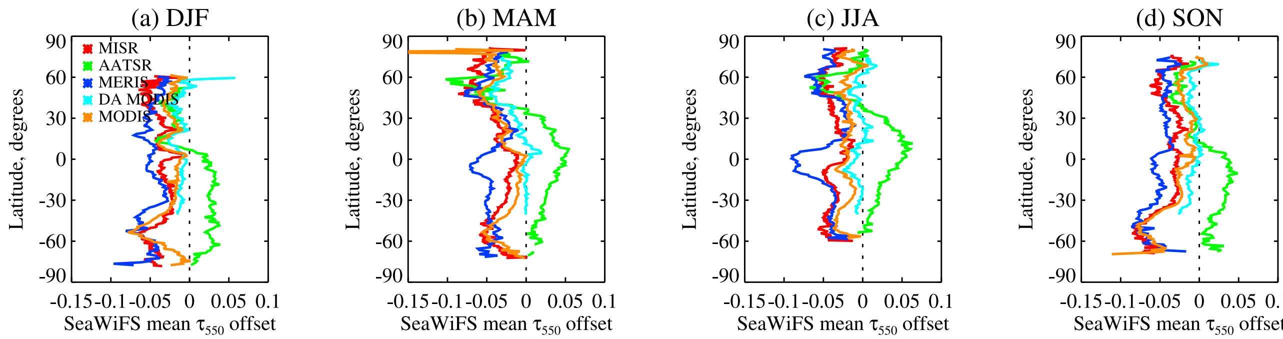

Figure 11. Zonal profiles of seasonal mean offset between SeaWiFS AOD at 550 nm and that from other sensors, defined such that positive values indicate SeaWiFS retrieves higher AOD. Calculated from Figure 10, for those latitude ranges with at least twenty points contributing to the zonal mean. Seasons are (a) DJF, (b) MAM, (c) JJA, and (d) SON. The dashed black line indicates zero difference. The MODIS and DA MODIS data shown are for Aqua only.

SeaWiFS-MISR bias in Table 3, the statistics become similar to those with the DA MODIS products, with excellent agreement overall, and the remaining SeaWiFS low bias is similar to that identified by comparison of SeaWiFS to AERONET data (of order −0.01). The same is true of the MODIS Collection 5.1 data, when high biases for low AODs of 0.01–0.015 identified by *Remer et al.* [2008] are removed.

[59] The AATSR data exhibit slightly lower correlation with SeaWiFS than for MODIS/MISR. A combination of small orbital overlap and stricter cloud screening in the AATSR product, which removes some high-AOD events, results in few high-AOD grid cells in the comparison. The total number of matched data pairs is also significantly smaller than for the other sensors. SeaWiFS has a high relative bias compared to AATSR at 550 nm (the majority of the data are for low-AOD points) and almost zero bias at 865 nm. SeaWiFS shows a better agreement at 865 nm with AATSR than with the other data sets considered, although the correlation is highest with MISR, perhaps due to the inclusion of more high-AOD events. Validation of this version of the AATSR algorithm against AERONET has not to date been performed globally and was therefore performed using the same protocol as for the SeaWiFS validation. For AATSR, Pearson's correlation coefficient R was 0.90 at 550 nm and 0.89 at 870 nm, and the lines of best fit at these wavelengths were $\tau_{\mathrm{AATSR},550} = 1.12\tau_{\mathrm{A},550} - 0.01$ and $\tau_{\mathrm{AATSR},870} = 1.1\tau_{\mathrm{A},870}$; the expected errors (again calculated as for SeaWiFS) were $0.03 + 0.12\tau_{\mathrm{A},550}$ and $0.02 + 0.2\tau_{\mathrm{A},870}$. These results indicate performance comparable to SeaWiFS.

[60] MERIS and SeaWiFS share the weakest correlations. Like SeaWiFS, MERIS was primarily designed as an ocean color sensor (and the original purpose of the MERIS aerosol retrieval considered here was for atmospheric correction of ocean color imagery) and lacks bands in the shortwave and thermal IR which are useful for cloud-flagging [*Antoine and Morel*, 1999]. The causes for the low correlation are believed twofold: first, there is a subset of points where SeaWiFS retrieves low AOD (less than 0.2) but MERIS retrieves a higher value, and second, there are few MERIS grid cells with $\tau_{550} \geq 0.6$. The relative high bias of SeaWiFS for high AODs as compared with other sensors is more extreme in the comparison with MERIS. This is consistent with the validation and intercomparison results of *Poulsen et al.* [2009].

[61] Figure 10 consists of seasonal composites of 550 nm SeaWiFS AOD for the 2005–2007 period, as well as maps of the seasonal mean difference between SeaWiFS and those sensors using the matched subsets of data in Figure 9. Zonal averages of these differences are presented in Figure 11. In both cases, plots for MODIS Terra are omitted as the spatial patterns match those of MODIS Aqua. The general similarity between the MISR and MODIS data is again evident. *Kahn et al.* [2009] compare colocated MISR and MODIS Terra retrievals extensively and identify a very strong agreement over ocean. Compared to MODIS and MISR, offsets between SeaWiFS and the DA MODIS data sets are closer to zero almost everywhere, although coverage is sparser and missing at high latitudes. Spatial patterns of difference are less consistent between the other data sets, although there are some commonalities, such as SeaWiFS AOD being persistently lower in the northern Atlantic Ocean (and to a lesser extent the northern Pacific). The reasons for this are unclear. Examination of Goddard Chemistry Aerosol Radiation and Transport (GOCART) model runs [*Chin et al.*, 2009] reveals the presence of transported Asian dust throughout the Northern hemisphere in springtime, with peak dust AODs at 550nm of around 0.05 (plus a similar AOD from non-dust sources), suggesting aerosol microphysical model choices could play a role here.

[62] Some seasonality in AOD differences is evident around aerosol outflow regions (e.g. African dust and biomass blowing), relating to differences in the strength of the aerosol events, and their seasonal movement. Some such events, such as African biomass burning late in the year, are missing from the composites, as there are few successful retrievals in one or both of the data sets in these regions.

[63] SeaWiFS retrieves a lower AOD than all other sensors except AATSR in the southern storm tracks. The DA MODIS data set does not include coverage in this region. Comparisons with MAN data by *Smirnov et al.* [2011] suggest that other data sets are biased high in this region, which may be due to the high cloudiness and wind speeds. Figure 7 shows a reasonable agreement between SeaWiFS and MAN in this region. However, the number of matchups is low in both cases. This could also explain some of the

differences in at high northern latitudes, although there are few MAN cruises in these regions. SeaWiFS and AATSR are closer in this region. Unlike the other satellite retrievals, the AATSR retrieval both takes into account wind speed when estimating surface reflectance, and retrieves surface albedo rather than prescribing it, although the directional behavior of surface reflectance is fixed. This means AATSR AOD retrievals are likely less susceptible than others to surface-reflectance-related errors in high-wind environments such as the storm tracks [*Sayer et al.*, 2010a].

[64] The DA MODIS data set removes many points around the intertropical convergence zone (ITCZ), most frequently suspected of contamination by thin cirrus. Interestingly, the offsets between SeaWiFS and MODIS/MISR are often closer to zero in this region than many others. *Pierce et al.* [2010] study the potential of MISR for retrieving cirrus optical depth and report that, particularly in the tropics, cirrus could not always be distinguished unambiguously from a mixture of dust and other aerosols. These results suggest that any cirrus-related bias in MODIS or MISR is likely also present in the SeaWiFS retrievals in these regions. This is not surprising, given SeaWiFS has a coarser spatial resolution than either and lacks both MODIS' near-IR (past 865 nm) and thermal IR bands, and MISR's multidirectional sampling. In contrast, SeaWiFS and other sensors are significantly lower than MERIS in this belt, which suggests that cirrus contamination could be more severe for MERIS.

5. Conclusions

[65] This study has described and validated an over-ocean aerosol optical depth retrieval algorithm (SOAR) from SeaWiFS data, which has been used in the creation of a new 13-year data set of spectral AOD. This represents the longest single-sensor record of total column AOD presently available from satellite measurements. Comparison with Sun photometer measurements reveals that the algorithm performs well. The fine mode volume fraction and Ångström exponent are able to distinguish between fine-dominated and coarse-dominated aerosol particle distributions for moderate and high AODs, although caution is required for low aerosol particle loadings. For general applications, use of only those retrievals with a quality assurance flag of 2 or 3 is recommended. The quality of the SeaWiFS data is similar to that of other satellite products, and the SeaWiFS aerosol data are suitable for quantitative scientific analysis.

[66] The data set has also been colocated and compared with a variety of other satellite AOD records, and the majority of the differences are consistent with known results based on each data set's validation efforts. This comparison also revealed a diversity in regional aerosol loading from different data sets. SOAR AODs are comparable to those from the existing OBPG SeaWiFS data set in clean conditions, and provide increased coverage in moderate and high aerosol loadings, such as dust storms.

[67] As mentioned in the Introduction, however, no current single-sensor data set can fill the requirements of a CDR, for reasons such as sampling and the inadequate information content of the measured radiances [e.g., *Mishchenko et al.*, 2007]. Additionally, changes in aerosol particle loading on timescales of individual sensor lifetimes are likely to be similar to the uncertainty of a satellite-derived trend [e.g., *Zhang and Reid*, 2010; *Platnick et al.*, 2011].

[68] In an effort to create a long-term multisensor consistent aerosol record, intersensor overlap will be crucial to assessing and correcting biases. In this regard, SeaWiFS occupies an important position. The SeaWiFS record coexisted with the earlier Advanced Very High Resolution Radiometer (AVHRR) and Along-Track Scanning Radiometer 2 (ATSR-2) records, and continued through the majority of the life of more recent Earth Observation systems (e.g. Terra, the A-Train, and Envisat). The high quality of radiometric accuracy through its lifetime makes it a useful bridge between different sensors.

[69] The SOAR algorithm could also be adapted for application to similar present or forthcoming sensors such as AVHRR, MODIS, or the Visible and Infrared Imager Radiometer Suite (VIIRS). Comparison with other aerosol data sets from these sensors would help to isolate the effects of algorithmic assumptions, and sensor-related (e.g. radiometric or sampling) differences between sensors on the derived aerosol property time series, and so help to pave the way for an eventual long-term CDR of the atmospheric aerosol particle loading.

[70] **Acknowledgments.** This work was supported by a grant from the NASA MEaSUREs program, managed by Martha Maiden. SeaWiFS level 1a data, the SeaDAS software, and NCEP meteorological fields were obtained from the SeaWiFS Ocean Biology Processing Group data distribution service. GlobAerosol was an ESA Data User Element project. The Naval Research Laboratory are thanked for the DA-MODIS data. MODIS data were obtained from the NASA LAADS, and MISR from the NASA Langley ASDC. The AERONET and MAN PIs are thanked for the creation and maintenance of the Sun photometer data records. The authors thank M. Chin, T. Diehl, R. A. Kahn, R. C. Levy, S. Mattoo, L. A. Remer, and Q. Tan for helpful discussions and comments on the manuscript. The authors acknowledge the detailed and constructive comments of three anonymous reviewers, whose suggestions strengthened the manuscript.

References

Ahmad, Z., B. A. Franz, C. R. McClain, E. J. Kwiatowska, J. Werdell, E. P. Shettle, and B. N. Holben (2010), New aerosol models for the retrieval of aerosol optical thickness and normalized water-leaving radiances from the SeaWiFS and MODIS sensors over coastal regions and open oceans, *Appl. Opt.*, *49*(29), 5545–5560, doi:10.1364/AO.49.005545.

Anderson, T. L., R. J. Charlson, D. M. Winker, J. A. Ogren, and K. Holmén (2003), Mesoscale variations of tropospheric aerosols, *J. Atmos. Sci.*, *60*, 119–136.

Anguelova, M., and F. Webster (2006), Whitecap coverage from satellite measurements: A first step toward modeling the variability of ocean whitecaps, *J. Geophys. Res.*, *111*, C03017, doi:10.1029/2005JC003158.

Antoine, D., and A. Morel (1999), A multiple scattering algorithm for atmospheric correction of remotely sensed ocean colour (MERIS instrument): Principle and implementation for atmospheres carrying various aerosols including absorbing ones, *Int. J. Remote Sens.*, *20*, 1875–1916.

Chin, M., T. Diehl, O. Dubovik, T. F. Eck, B. N. Holben, A. Sinyuk, and D. G. Streets (2009), Light absorption by pollution, dust, and biomass burning aerosols: A global model study and evaluation with AERONET measurements, *Ann. Geophys.*, *27*, 3439–3464, doi:10.5194/angeo-27-3439-2009.

Cox, C., and W. Munk (1954a), Statistics of the sea surface derived from Sun glitter, *J. Mar. Res.*, *13*, 198–227.

Cox, C., and W. Munk (1954b), Measurement of the roughness of the sea surface from photographs of the Sun's glitter, *J. Opt. Soc. Am.*, *44*, 838–850, doi:10.1364/JOSA.44.000838.

Dave, J. V. (1976), Investigation of the effect of atmospheric dust on the determination of total ozone from the Earth's ultraviolet reflectivity measurements, *Tech. Rep. NASA-CR-152-516*, 134 pp., IBM, Gaithersburg, Md.

Derber, J. C., D. F. Parrish, and S. Lord (1991), The new global operational analysis system at the National Meteorological Center, *Weather Forecasting*, *6*, 538–547.

Dubovik, O., and M. D. King (2000), A flexible inversion algorithm for retrieval of aerosol optical properties from Sun and sky radiance measurements, *J. Geophys. Res.*, *105*, 20,673–20,696, doi:10.1029/2000JD900282.

Dubovik, O., et al. (2006), The application of spheroid models to account for aerosol particle non-sphericity in remote sensing of desert dust, *J. Geophys. Res.*, *111*, D11208, doi:10.1029/2005JD006619.

Eck, T. F., B. N. Holben, J. S. Reid, O. Dubovik, A. Smirnov, N. T. O'Neill, I. Slutsker, and S. Kinne (1999), Wavelength dependence of the optical depth of biomass burning, urban, and desert dust aerosols, *J. Geophys. Res.*, *104*(D24), 31,333–31,349.

Eplee, R. E., Jr., F. S. Patt, R. A. Barnes, and C. R. McClain (2007), SeaWiFS long-term solar diffuser reflectance and sensor noise analyses, *Appl. Opt.*, *46*, 762–773, doi:10.1364/AO.46.000762.

Eplee, R. E., Jr., J.-Q. Sun, G. Meister, F. S. Patt, X. Xiong, and C. R. McClain (2011), Cross calibration of SeaWiFS and MODIS using on-orbit observations of the Moon, *Appl. Opt.*, *50*(2), 120–133, doi:10.1364/AO.50.000120.

Forster, P., et al. (2007), Changes in atmospheric constituents and in radiative forcing, in *Climate Change 2007, the Physical Science Basis. Contribution of Working Group 1 to the Fourth Assessment Report of the Intergovernmental Panel on Climate Change*, pp. 129–234, Cambridge Univ. Press, Cambridge, U. K.

Franz, B. A., S. W. Bailey, P. J. Werdell, and C. R. McClain (2007), Sensor-independent approach to the vicarious calibration of satellite ocean color radiometry, *Appl. Opt.*, *46*(22), 5068–5082, doi:10.1364/AO.46.005068.

Global Climate Observing System (GCOS) (2009), Guideline for the generation of satellite-based datasets and products meeting GCOS requirements, *WMO/TD 1488*, World Meteorol. Org., Geneva, Switzerland.

Global Climate Observing System (GCOS) (2010), Implementation plan for the global observing system for climate in support of the UNFCC, *WMO/TD 1244*, World Meteorol. Org., Geneva, Switzerland.

Hasekamp, O. P., and J. Landgraf (2007), Retrieval of aerosol properties over land surfaces: Capabilities of multi-viewing-angle intensity and polarization measurements, *Appl. Opt.*, *46*(16), 3332–3344, doi:10.1364/AO.46.003332.

Holben, B. N., et al. (1998), AERONET: A federated instrument network and data archive for aerosol characterization, *Remote Sens. Environ.*, *66*, 1–16, doi:10.1016/S0034-4257(98)00031-5.

Hsu, N. C., S.-C. Tsay, M. D. King, and J. R. Herman (2004), Aerosol properties over bright-reflecting source regions, *IEEE Trans. Geosci. Remote Sens.*, *42*(3), 557–569, doi:10.1109/TGRS.2004.824067.

Hsu, N. C., S.-C. Tsay, M. D. King, and J. R. Herman (2006), Deep Blue retrievals of Asian aerosol properties during ACE-Asia, *IEEE Trans. Geosci. Remote Sens.*, *44*(11), 3180–3195, doi:10.1109/TGRS.2006.879540.

Huang, J., N. C. Hsu, S.-C. Tsay, M. J. Jeong, B. N. Holben, T. A. Berkoff, and E. J. Welton (2011), Susceptibility of aerosol optical thickness retrievals to thin cirrus contamination during the BASE-ASIA campaign, *J. Geophys. Res.*, *116*, D08214, doi:10.1029/2010JD014910.

Hyer, E. H., J. S. Reid, and J. Zhang (2011), An over-land aerosol optical depth data set for data assimilation by filtering, correction, and aggregation of MODIS Collection 5 optical depth retrievals, *Atmos. Meas. Tech.*, *4*, 379–408, doi:10.5194/amt-4-379-2011.

Ichoku, C., D. A. Chu, S. Mattoo, Y. J. Kaufman, L. A. Remer, D. Tanré, I. Slutsker, and B. N. Holben (2002), A spatio-temporal approach for global validation and analysis of MODIS aerosol products, *Geophys. Res. Lett.*, *29*(12), 8006, doi:10.1029/2001GL013206.

Jamet, C., H. Loisel, C. P. Kuchinke, K. Ruddick, G. Zibordi, and H. Feng (2011), Comparison of three SeaWiFS atmospheric correction algorithms for turbid waters using AERONET-OC measurements, *Remote Sens. Environ.*, *115*(8), 1955–1965, doi:10.1016/j.rse.2011.03.018.

Kahn, R. A., D. L. Nelson, M. J. Garay, R. C. Levy, M. A. Bull, D. J. Diner, J. V. Martonchik, S. R. Paradise, E. G. Hansen, and L. A. Remer (2009), MISR aerosol product attributes and statistical comparisons with MODIS, *IEEE Trans. Geosci. Remote Sens.*, *47*(12), 4095–4114, doi:10.1109/TGRS.2009.2023115.

Kahn, R. A., B. J. Gaitley, M. J. Garay, D. J. Diner, T. F. Eck, A. Smirnov, and B. N. Holben (2010), Multiangle Imaging SpectroRadiometer global aerosol product assessment by comparison with the Aerosol Robotic Network, *J. Geophys. Res.*, *115*, D23209, doi:10.1029/2010JD014601.

Kahn, R. A., M. J. Garay, D. L. Nelson, R. C. Levy, M. A. Bull, D. J. Diner, J. V. Martonchik, E. G. Hansen, L. A. Remer, and D. Tanré (2011), Response to 'Toward unified satellite climatology of aerosol properties: 3. MODIS versus MISR versus AERONET', *J. Quant. Spectrosc. Radiat. Transfer*, *112*(5), 901–909, doi:10.1016/j.jqsrt.2010.11.001.

Kalashnikova, O. V., R. Kahn, I. N. Sokolik, and W.-H. Li (2005), Ability of multiangle remote sensing observations to identify and distinguish mineral dust types: Optical models and retrievals of optically thick plumes, *J. Geophys. Res.*, *110*, D18S14, doi:10.1029/2004JD004550.

Kaufman, Y. J., I. Koren, L. A. Remer, D. Tanré, P. Ginoux, and S. Fan (2005), Dust transport and deposition observed from the Terra-Moderate Resolution Imaging Spectroradiometer (MODIS) spacecraft over the Atlantic Ocean, *J. Geophys. Res.*, *110*, D10S12, doi:10.1029/2003JD004436.

Knobelspiesse, K. D., C. Pietras, G. S. Fargion, M. Wang, R. Frouin, M. A. Miller, A. Subramaniam, and W. M. Balch (2004), Maritime aerosol optical thickness measured by handheld Sun photometers, *Remote Sens. Environ.*, *93*(1–2), 87–106, doi:10.1016/j.rse.2004.06.018.

Koepke, P. (1984), Effective reflectance of oceanic whitecaps, *Appl. Opt.*, *23*(11), 1816–1824, doi:10.1364/AO.23.001816.

Kokhanovsky, A. A., et al. (2010), The determination of spectral aerosol optical thickness from satellites: An inter-comparison of algorithms using synthetic backscattered solar light characteristics, *Atmos. Meas. Tech.*, *3*, 909–932, doi:10.5194/amt-3-909-2010.

Kotchenova, S. Y., E. F. Vermote, R. Levy, and A. Lyapustin (2008), Radiative transfer codes for atmospheric correction and aerosol retrieval: Intercomparison study, *Appl. Opt.*, *47*, 2215–2226, doi:10.1364/AO.47.002215.

Levenberg, K. (1944), A method for the solution of certain non-linear problems in least-squares, *Q. Appl. Math.*, *2*(2), 164–168.

Levy, R. C., G. G. Leptoukh, R. Kahn, V. Zubko, A. Gopalan, and L. A. Remer (2009), A critical look at deriving monthly aerosol optical depth from satellite data, *IEEE Trans. Geosci. Remote Sens.*, *47*(8), 2942–2956, doi:10.1109/TGRS.2009.2013842.

Levy, R. C., L. A. Remer, R. G. Kleidman, S. Mattoo, C. Ichoku, R. Kahn, and T. F. Eck (2010), Global evaluation of the Collection 5 MODIS dark-target aerosol products over land, *Atmos. Chem. Phys.*, *10*, 10,399–10,420, doi:10.5194/acp-10-10399-2010.

Marquardt, D. R. (1963), An algorithm for the least-squares estimation of nonlinear parameters, *SIAM J. Appl. Math.*, *11*(2), 431–441, doi:10.2307/2098941.

Martins, J. V., D. Tanré, L. Remer, Y. Kaufman, S. Mattoo, and R. Levy (2002), MODIS cloud screening for remote sensing of aerosols over oceans using spatial variability, *Geophys. Res. Lett.*, *29*(12), 8009, doi:10.1029/2001GL013252.

Martonchik, J. V., D. J. Diner, R. A. Kahn, T. P. Ackerman, M. M. Verstraete, B. Pinty, and H. R. Gordon (1998), Techniques for the retrieval of aerosol properties over land and ocean using multiangle imaging, *IEEE Trans. Geosci. Remote Sens.*, *36*(4), 1212–1227, doi:10.1109/36.701027.

Martonchik, J. V., R. A. Kahn, and D. J. Diner (2009), Retrieval of aerosol properties over land using MISR observations, in *Aerosol Remote Sensing Over Land*, edited by A. Kokhanovsky and G. de Leeuw, pp. 267–293, Springer, Berlin.

McClain, C. R., G. C. Feldman, and S. B. Hooker (2004), An overview of the SeaWiFS project and strategies for producing a climate research quality global ocean bio-optical time series, *Deep Sea Res.*, *51*, 5–42, doi:10.1016/j.dsr2.2003.11.001.

McClatchey, R. A., R. W. Fenn, J. E. A. Selby, F. E. Volz, and J. S. Garing (1971), Optical properties of the atmosphere (revised), *Tech. Rep. AFCRL-TR-71-0279*, 354 pp., Air Force Cambridge Res. Lab., Cambridge, Mass.

Mishchenko, M., L. D. Travis, and D. W. Mackowski (1996), T-matrix computations of light scattering by nonspherical particles: A review, *J. Quant. Spectrosc. Radiat. Transfer*, *55*, 535–575, doi:10.1016/0022-4073(96)00002-7.

Mishchenko, M. I., I. V. Geogdzhayev, B. Cairns, B. E. Carlson, J. Chowdhary, A. A. Lacis, L. Liu, W. B. Rossow, and L. D. Travis (2007), Past, present, and future of global aerosol climatologies derived from satellite observations: A perspective, *J. Quant. Spectrosc. Radiat. Transfer*, *106*, 325–347, doi:10.1016/j.jqsrt.2007.01.007.

Morel, A., and L. Prieur (1977), Analysis of variations in ocean color, *Limnol. Oceanogr.*, *22*(4), 709–722.

Pierce, J. R., R. A. Kahn, M. R. Davis, and J. M. Comstock (2010), Detecting thin cirrus in Multiangle Imaging Spectroradiometer aerosol retrievals, *J. Geophys. Res.*, *115*, D08201, doi:10.1029/2009JD013019.

Platnick, S., A. Amarasinghe, and the MODIS Atmosphere Team (2011), Climate data records: A MODIS perspective, paper presented at Workshop on Observations and Modeling of Aerosol/Cloud Properties for Climate Studies, Univ. Lille, Paris.

Poulsen, C. A., R. Siddans, G. E. Thomas, A. Sayer, R. G. Grainger, O. Perez-Navarro, O. Portela-Arjona, and P. Yves-Deschamps (2009), ESA GlobAerosol: Final validation and intercomparison report, version 3.2, technical report, Eur. Space Agency, Paris. [Available from http://www.globaerosol.info/docs/globaer_vir_v3p2.pdf.]

Remer, L. A., D. Tanré, and Y. J. Kaufman (2006), Algorithm for remote sensing of tropospheric aerosol from MODIS: Collection 5, *Tech. Rep. ATBD-MOD-02*, NASA Goddard Space Flight Center, Greenbelt, Md. [Available at http://modis.gsfc.nasa.gov/data/atbd/.]

Remer, L. A., et al. (2008), Global aerosol climatology from the MODIS satellite sensors, *J. Geophys. Res.*, *113*, D14S07, doi:10.1029/2007JD009661.

Rodgers, C. D. (2000), *Inverse Methods for Atmospheric Sounding: Theory and Practice*, *Ser. Atmos. Oceanic Planet. Phys.*, vol. 2, World Sci., Hoboken, N. J.

Sayer, A. M., G. E. Thomas, and R. G. Grainger (2010a), A sea surface reflectance model for (A)ATSR, and application to aerosol retrievals, *Atmos. Meas. Tech.*, *3*, 813–838, doi:10.5194/amt-3-813-2010.

Sayer, A. M., G. E. Thomas, P. I. Palmer, and R. G. Grainger (2010b), Some implications of sampling choices on comparisons between satellite and model aerosol optical depth fields, *Atmos. Chem. Phys.*, *10*, 10,705–10,716, doi:10.5194/acp-10-10705-2010.

Sayer, A. M., A. Smirnov, N. C. Hsu, and B. N. Holben (2012), A pure marine aerosol model, for use in remote sensing applications, *J. Geophys. Res.*, doi:10.1029/2011JD016689, in press.

Shi, Y., J. Zhang, J. S. Reid, B. N. Holben, E. J. Hyer, and C. Curtis (2011), An analysis of the collection 5 MODIS over-ocean aerosol optical depth product for its implication in aerosol assimilation, *Atmos. Chem. Phys.*, *11*, 557–565, doi:10.5194/acp-11-557-2011.

Smirnov, A., B. N. Holben, T. F. Eck, O. Dubovik, and I. Slutsker (2000), Cloud-screening and quality control algorithms for the AERONET database, *Remote Sens. Environ.*, *73*(3), 337–349.

Smirnov, A., B. N. Holben, Y. J. Kaufman, O. Dubovik, T. F. Eck, I. Slutsker, C. Pietras, and R. H. Halthore (2002), Optical properties of atmospheric aerosol in maritime environments, *J. Atmos. Sci.*, *59*, 501–523.

Smirnov, A., et al. (2009), Maritime aerosol network as a component of aerosol robotic network, *J. Geophys. Res.*, *112*, D06204, doi:10.1029/2008JD011257.

Smirnov, A., et al. (2011), Maritime Aerosol Network as a component of AERONET-first results and comparison with global aerosol models and satellite retrievals, *Atmos. Meas. Tech.*, *4*, 583–597, doi:10.5194/amt-4-583-2011.

Stevens, B., and G. Feingold (2009), Untangling aerosol effects on clouds and precipitation in a buffered system, *Nature*, *461*, 607–613, doi:10.1038/nature08281.

Stramska, M., and T. Petelski (2003), Observations of oceanic whitecaps in the north polar waters of the Atlantic, *J. Geophys. Res.*, *108*(C3), 3086, doi:10.1029/2002JC001321.

Tanré, D., M. Herman, and Y. J. Kaufman (1996), Information on aerosol size distribution contained in solar reflected spectral radiances, *J. Geophys. Res.*, *101*(D14), 19,043–19,060.

Tanré, D., Y. J. Kaufman, M. Herman, and S. Mattoo (1997), Remote sensing of aerosol properties over oceans using the MODIS/EOS spectral radiances, *J. Geophys. Res.*, *102*(D14), 16,971–16,988, doi:10.1029/96JD03437.

Thomas, G. E., C. A. Poulsen, A. M. Sayer, S. H. Marsh, S. M. Dean, E. Carboni, R. Siddans, and R. G. Grainger (2009), Oxford-RAL Aerosol and Cloud (ORAC): Aerosol retrievals from satellite radiometers, in *Aerosol Remote Sensing Over Land*, edited by A. A. Kokhanovsky and G. de Leeuw, pp. 193–225, Springer, Berlin.

Thuillier, G., M. Hersé, P. C. Simon, D. Labs, H. Mandel, D. Gillotay, and T. Foujols (2003), The solar spectral irradiance from 200 to 2400 nm as measured by the SOLSPEC spectrometer from the ATLAS 1-2-3 and EURECA missions, *Sol. Phys.*, *214*(1), 1–22.

Vermote, E. F., D. Tanré, J. L. Deuzé, M. Herman, and J.-J. Morcrette (1997), Second Simulation of the Satellite Signal in the Solar Spectrum, 6S: An overview, *IEEE Trans. Geosci. Remote Sens.*, *35*(3), 675–686, doi:10.1109/36.581987.

Wagner, F., and A. M. Silva (2008), Some considerations about Ångström exponent distributions, *Atmos. Chem. Phys.*, *8*, 481–489, doi:10.5194/acp-8-481-2008.

Zhang, J., and J. S. Reid (2006), MODIS aerosol product analysis for data assimilation: Assessment of over-ocean level 2 aerosol optical thickness retrievals, *J. Geophys. Res.*, *111*, D22207, doi:10.1029/2005JD006898.

Zhang, J., and J. S. Reid (2010), A decadal regional and global trend analysis of the aerosol optical depth using a data-assimilation grade over-water MODIS and Level 2 MISR aerosol products, *Atmos. Chem. Phys.*, *10*, 10,949–10,963, doi:10.5194/acp-10-10949-2010.

Z. Ahmad, C. Bettenhausen, B. N. Holben, N. C. Hsu, A. M. Sayer, and A. Smirnov, NASA Goddard Space Flight Center, Greenbelt, MD 20771, USA. (andrew.sayer@nasa.gov)

G. E. Thomas, Atmospheric, Oceanic, and Planetary Physics, University of Oxford, Parks Road, Oxford OX1 3PU, UK.

J. Zhang, Department of Atmospheric Science, University of North Dakota, Grand Forks, ND 58202, USA.